Phase dynamics in graphene-based Josephson junctions in the presence of thermal and correlated fluctuations

Claudio Guarcello,[1,2,*] Davide Valenti,[1,†] and Bernardo Spagnolo[1,2,3,‡]

[1]*Dipartimento di Fisica e Chimica, Group of Interdisciplinary Theoretical Physics, Università di Palermo and CNISM, Unità di Palermo, Viale delle Scienze, Edificio 18, 90128 Palermo, Italy*

[2]*Radiophysics Department, Lobachevsky State University, Nizhny Novgorod, Russia*

[3]*Istituto Nazionale di Fisica Nucleare, Sezione di Catania, Italy*

(Received 15 August 2015; published 17 November 2015)

We study by numerical methods the phase dynamics in ballistic graphene-based short Josephson junctions. A superconductor-graphene-superconductor system exhibits superconductive quantum metastable states similar to those present in normal current-biased Josephson junctions. We investigate the effects of thermal and correlated fluctuations on the escape time from these metastable states, when the system is driven by an oscillating bias current in the presence of Gaussian white and colored noise sources. Varying the intensity and the correlation time of the noise source, it is possible to analyze the behavior of the escape time, or switching time, from a superconductive metastable state in different temperature regimes. Moreover, we are able to clearly distinguish dynamical regimes characterized by the dynamic resonant activation effect, in the absence of noise source, and the stochastic resonant activation phenomenon induced by the noise. For low initial values of the bias current, the dynamic resonant activation shows double-minimum structures, strongly dependent on the value of the damping parameter. Noise-enhanced stability is also observed in the system investigated. We analyze the probability density function (PDF) of the switching times. The PDFs for frequencies within the dynamic resonant activation minima are characterized by single peaks with exponential tails. The PDFs for noise intensities around the maxima of the switching time, peculiarity of the noise-enhanced stability phenomenon, are composed of regular sequences of two peaks for each period of the driving current, with exponentially decaying envelopes.

DOI: 10.1103/PhysRevB.92.174519 PACS number(s): 85.25.Cp, 81.05.ue, 05.10.Gg, 72.70.+m

I. INTRODUCTION

The possibility of obtaining graphene [1] by extraction of single layers from graphite paved the way for a new generation of superconductive graphene-based devices. The charge carriers in graphene are massless quasiparticles, the Dirac fermions, with pseudospin half and linear energy dispersion. The band structure shows contact points, called Dirac points, between the conduction and valence bands [2]. These peculiar electronic properties give rise to interesting phenomena, such as specular Andreev reflection [2,3], unusual propagating modes along graphene channels [4], and oscillatory dependence of the Josephson current on the barrier thickness and applied bias voltage [5]. The refractoriness of graphene to the surface oxidation in a natural environment favors the realization of highly transparent contacts with the superconductive electrodes. Furthermore, superconductivity in graphene, pure or doped, was predicted and explored [6,7] and new devices, as dc SQUIDs [8,9], proximity Josephson sensors [10], or bolometers based on superconductive tunnel junction contacts [11], were fabricated using graphene.

Superconducting states in graphene have been experimentally realized by the proximity effect through contact with superconducting electrodes [12–14], indicating coherent propagation of Cooper pairs in graphene. This experimental evidence raises the question of whether it would be possible to modify graphene to become an intrinsic superconductor. In fact, there have been several theoretical attempts to understand intrinsic superconductivity in graphene [6,15–19]. Uchoa *et al.* [6], within the mean-field approach, suggested two singlet pairing states, s wave and an exotic $p+ip$ due to the special structure of the honeycomb lattice. Honerkmap *et al.* [16], considering a nearest-neighbor spin-spin interaction, found that doping away from half filling can lead to a $d+id$ superconducting state. The $d+id$ superconducting state is also supported by mean-field study [17] and Monte Carlo approaches [18,19].

On the other side, proximity-induced superconductivity is per se an intriguing feature which has received considerable attention after Beenakker's result (for a review see Ref. [20]). Several experimental works observed proximity-induced supercurrent between two superconducting electrodes on top of a graphene monolayer [12–14,21,22], so that the theoretical interest in superconductor-graphene-superconductor (SGS) structures significantly increased.

In particular, in the limit of zero temperature, the behavior of critical current and current-phase relationship (CΦR) in the limit of the *short ballistic* SGS system (where the junction length L is smaller than both the junction width W and the superconducting coherence length ξ) was studied by Titov and Beenakker [23]. Taking a cue from these results, Lambert *et al.* [24] derived a washboard potential for a suspended graphene junction. The phase, the temperature, and the junction length dependence of the supercurrent for the ballistic SGS junction was finally calculated by Hagimásy *et al.* [25].

Approaches in Refs. [23,25] use the Dirac–Bogoliubov–de Gennes (DBdG) formalism, assuming isotropic s-wave pairing in the superconductors. The equation however could be modified and adapted to the case of anisotropic wave pairing,

*claudio.guarcello@unipa.it
†davide.valenti@unipa.it
‡bernardo.spagnolo@unipa.it

TABLE I. Experimental values of different JJ parameters, calculated or directly acquired by various published papers [12,13,36–39].

		Mizuno [36]	Coskun [38]	Du [13]	Heerschee [12]	English [39] Samples A/B/C/D	Miao [37]
I_c	(nA)	100	10^4	800	10	71/107 39/160	110
β_C		76	16				
C	(pF)	1	[12,50]				
R_N	(Ω)	500	10				
T	(K)	3	0.4	0.2	0.3	0.01	0.3
T_{co}	(K)	0.02	$[26,54]\times10^{-3}$				[0.12,1.2]
γ^c		1.3	1.7×10^{-3}	0.01	1.3	6/4/11/3 $\times10^{-3}$	0.11
ω_{p_0}	(GHz)	17	[25,50]				$[10^2,10^3]$

relevant for theoretical proposals of the intrinsic superconductivity in graphene [6,15–19]. As a result, modifications of the CΦR are expected, which should influence the switching dynamics from the superconducting metastable state to the resistive one.

Titov [23] and Hagimásy [25] solved the DBdG equation in an impurity-free SGS junction. The experimental results of Heersche [12] for a graphene-based Josephson junction (JJ) are qualitatively similar to the theoretical prediction of Ref. [23], but with remarkable quantitative differences. In fact, the experimental value of the I_cR_N product at the Dirac point significantly deviates from the theoretical prediction, and the increase of I_cR_N at higher carrier densities is much larger than predicted. However this discrepancy is not due to the intrinsic electron-phonon (e-ph) mechanism, but, according to Beenakker [20], can be likely related to disorder in the experimental sample, which is not included in the calculation [13].

It is quite established that electron-phonon coupling, which is important analyzing the diffusion in heterostructures [26], becomes exceedingly small near the Dirac point in graphene [27–33]. It is therefore arguable that the diversion of the above theoretical results from experimental findings cannot have any sizable contribution from the lattice degree of freedom, i.e., from phonon excitations, at least compared to other contributions. Moreover, the restrictions in energy transfer caused by momentum conservation are responsible for the weak electron–acoustic phonon coupling in graphene [33]. In fact, the maximum change of momentum at the Fermi level is twice the Fermi momentum $2k_F$, which corresponds to phonon energy $\hbar\omega_{2k_F}$. This energy defines a characteristic temperature, the *Bloch-Grüneisen temperature*, by $\omega_{2k_F} = kT_{BG}$, above which only a fraction of phonons is available for scattering with electrons in the thermal window. Manifestations of this effect have been observed in resistance versus temperature measurements [34], especially on electrolytically gated graphene [35]. The scattering probability, which is proportional to the number of thermally excited phonons, is therefore negligible at $T \ll T_{BG}$ (see Eq. (11.110) of Ref. [33]). Up to room temperature, this excludes also all optical phonons in graphene from our consideration (for a detailed description of the scattering processes in suspended graphene see Chap. 11.4 of Ref. [33]). In particular, the values of T_{BG} shown in Fig. 3(b) of Ref. [35], as a function of the carrier density, are always greater than ∼100 K. These temperatures are definitively above the temperatures at which graphene-based JJs commonly work (see Table I and Refs. [12,13,36–39] therein). As a consequence, the e-ph scattering is neglected.

The ballistic nature of graphene-based Josephson junctions was demonstrated in both suspended [36] and vertical [40] junction geometries.

A Josephson junction is a mesoscopic system in which macroscopic quantities, such as as current and voltage, are directly dependent on the transient dynamics of a microscopic order parameter [41,42]. Moreover, JJs are typical out-of-equilibrium systems characterized by tilted or switching periodic potentials [43,44]. The output of this device is strongly affected by environmental perturbations, that is, stochastic fluctuations of temperature, current, or magnetic field. Different aspects of graphene-based junctions in a noisy environment were already examined by several authors. Miao *et al.* [37] took into account the noise-induced premature switching in underdamped SGS JJs at finite temperature. Specifically, in Ref. [37] the reduction of the critical current I_c and variations in the product I_cR_N were experimentally observed and theoretically explained considering the thermal fluctuations nonnegligible (R_N is the normal resistance of the junction).

Other authors [13,45] suggested a supercurrent reduction by premature switching induced by thermal and electromagnetic noise. Coskun *et al.* [38] studied the thermally activated dynamics of phase slip in SGS JJs through the measurement of the switching current distribution. They found an anomalous temperature dependence of the switching current dispersion due to nontrivial structure [23,25] of the Josephson current. A simple stochastic model to analyze the electrodynamics of an underdamped graphene JJ was proposed by Mizuno *et al.* [36]. They stressed the importance of realizing high-quality suspended SGS structures, to prevent disorders due to the conventionally used substrates, whereby a flow of supercurrent at high critical temperature T_c can be obtained. The SGS junction is a good candidate for the fabrication of gate-tunable phase qubits [46,47]. In Ref. [46] the study of the stochastic switching-current distribution $P(I_c)$ in an SGS junction for low temperatures allowed highlighting the macroscopic quantum tunneling and energy level quantization, similarly to conventional

JJs. Moreover, Lee *et al.* [46] studied the switching-current distribution in both quantum and thermal regimes, building up a computational analysis based on the pure resistively and capacitively shunted junction (RCSJ) model for a conventional JJ [48,49]. Considering a range of temperatures in which the dynamics is exclusively ruled by thermal fluctuations, Lee *et al.* [46] observed disagreement between the experimental and fitted temperatures. The deviation in the temperature most likely occurs because the nonsinusoidal CΦR [23], exhibited in the SGS junction, was not used.

The work presented in this paper fits well into this scenario, since it aims to study how thermal fluctuations affect the dynamical behavior of an SGS junction. In particular, we study the influence of Gaussian (white or colored) noise sources on the switching dynamics from the superconductive metastable state to the resistive one in a suspended graphene-based short JJ, considering the proper CΦR [23]. Specifically, we focus on the *mean switching time* (MST) from the superconductive to the resistive regime. We recall that the effects of thermal fluctuations on the dynamics of conventional short [50–54] and long [55–59] JJs have been thoroughly investigated, both theoretically predicting [50–54,56,58–60] and experimentally observing [61–63] noise-induced effects in the superconductive lifetime of a JJ.

The rate of switching from the JJ metastable superconducting state encodes information about the noise present in an input signal [64–68]. The use of JJs as detectors, based on the statistics of the escape times, has been recently proposed [64–70]. Specifically, the statistical analysis of the switching events from the metastable superconducting state to the resistive running state of the JJ has been proposed to detect weak periodic signals embedded in a noisy environment [69–73].

In this paper we analyze the transient dynamics of an underdamped SGS junction, considering the simultaneous action of an external driving force oscillating with frequency ω, and a stochastic signal which represents a random force of intensity γ. We focus our analysis on the mean lifetime of the superconductive state. The study is performed fixing the initial values of the applied bias current i_0 and the correlation time τ_c of the colored noise source, and varying the frequency ω and the noise intensity γ. Whenever possible, results are compared with those obtained for conventional JJs, that is, a junction formed by a superconductor–"normal" nonsuperconductor–superconductor (SNS) structure.

The results of this work can be applied to the problem of a particle diffusing in a periodic "washboard" (e.g., sinusoidal) potential [74,75], a generic model with relevance in several areas different from the biased Josephson junction context, such as particle transport on topologically or energetically structured surfaces [76–78], magnetic domain-wall motion [79,80], motor proteins [81,82], particles in optical lattices and optical line traps [83–85], and more generally in biophysical processes [81,86–88].

The paper is organized as follows. The next section is an overview of the physical model. In Sec. III the theoretical results are shown and analyzed. Section IV contains a *probability density function* (PDF) analysis of the escape times, by focusing on the appearance of noise-induced nonmonotonic effects in the MST behavior. In Sec. V conclusions are drawn.

II. THE MODEL

The electrodynamics of a JJ can be analyzed looking at the time evolution of the order parameter φ, that is, the phase difference between the wave functions of the two coupled superconductors forming the device. According to the RCSJ model and including the environmental influence, the equation of motion for φ is

$$\varphi_{tt}(t) + \beta_J \varphi_t(t) = i_b(t) - i_\varphi(t) + i_f(t), \tag{1}$$

where $i_b(t)$ and $i_\varphi(t)$ are the bias and supercurrent, respectively, both normalized to the critical current of the junction I_c. The term $i_f(t)$, also normalized to I_c, represents the stochastic noise contribution. Hereafter, lowercase (uppercase) letters are used to indicate normalized (nonnormalized) current terms with respect to the critical value I_c. The subscripts of φ denote partial derivatives in time. The use of normalized variables allows us to extend, in a direct and simple way, the theoretical results to different experimental settings. Equation (1) is in accordance with the Johnson approach [48], since it includes a damping parameter $\beta_J = (\omega_{p_0} R_N C)^{-1}$, multiplied by $\varphi_t(t)$, and assumes the time variable normalized to the inverse of the zero-bias plasma frequency $\omega_{p_0} = \sqrt{2\pi I_c/(\Phi_0 C)}$. Here, C is the capacitance of the junction and $\Phi_0 = h/2e$ is the magnetic flux quantum (e is the electron charge and h is Planck's constant). Introducing the parameter $\beta_C = {\beta_J}^{-2}$, Eq. (1) can be alternatively arranged in the Stewart-McCumber framework [48], according to which a term $\beta_C \varphi_{tt}(t)$ is included in the equation, and the time variable is normalized to the inverse of the JJ characteristic frequency $\omega_c = \omega_{p_0}^2 R_N C$. The dynamics of a JJ can be described as the motion of a "phase particle" with mass $m = C(\Phi_0/2\pi)^2$ rolling down along the profile of a potential, called the *washboard potential*, composed of a tilted sequence of wells.

For a conventional current biased junction SNS, the normalized supercurrent and washboard potential have the well-known expressions

$$i_\varphi(t) = \sin[\varphi(t)], \tag{2}$$

$$U(\varphi,t) = -E_J\{\cos[\varphi(t)] + i_b(t)\,\varphi(t)\}, \tag{3}$$

where $E_J = \Phi_0 I_c/2\pi$ is the Josephson coupling energy, that is, the energy initially stored in the junction. The bias current represents the slope of this potential. Equation (2) is the *dc Josephson relation* [41,42]. In the limit of small-amplitude oscillations, the JJ plasma frequency corresponds to the oscillation frequency in the bottom of a potential well [49], modified by the presence of a bias current according to

$$\omega_P(t) = \sqrt{\frac{1}{m}\frac{d^2U}{d\varphi^2}\bigg|_{\varphi_{\min}}} = {\omega_{p_0}}^4\sqrt{1 - i_b^2(t)}, \tag{4}$$

where $\varphi_{\min} = \arcsin[i_b(t)]$ is the value of the order parameter at a minimum of $U(\varphi,t)$. Titov and Beenakker [23] calculated the CΦR and critical current for a ballistic graphene-based junction at the Dirac point. They addressed the problem in the framework of the DBdG equation [3,89]. Considering the

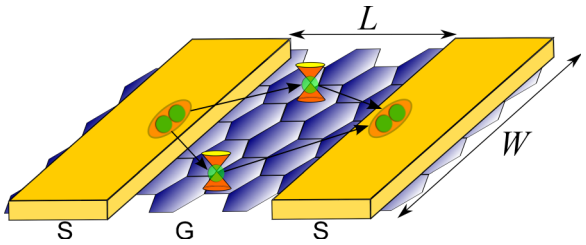

FIG. 1. (Color online) Schematic view of a suspended SGS device. The electrons forming a Cooper pair, when they enter graphene, move into different K valleys, represented as orange cones. In the short-junction regime, $L \ll W$.

Josephson current at zero temperature [90]

$$I(\varphi) = -\frac{4e}{\hbar}\frac{d}{d\varphi}\int_0^\infty d\varepsilon \sum_{n=0}^{\infty} \rho_n(\varepsilon,\varphi)\varepsilon, \tag{5}$$

supposing an "ideal" normal metal–superconductor interface, and taking hard wall boundary conditions [38,91], they obtained the following expressions:

$$i_\varphi(t) = \frac{I(\varphi)}{I_c} = \frac{2}{1.33}\cos\left(\frac{\varphi}{2}\right)\tanh^{-1}\left[\sin\left(\frac{\varphi}{2}\right)\right], \tag{6}$$

$$I_c = 1.33\frac{e\Delta_0}{\hbar}\frac{W}{\pi L}, \tag{7}$$

where W and L are the linear dimensions of the device (see Fig. 1), that is, the length of the superconductive plates and their separation, respectively. Furthermore Δ_0 is the superconductive excitation gap and $\hbar = h/2\pi$. Equations (6) and (7) refer to junctions with short and wide normal region, that is $L \ll W$, and to the *short-junction* regime, in which L is smaller than the superconducting coherence length ξ, describing the spatial spread of Cooper-paired electrons. We recall that the simple CΦR given in Eq. (6) is obtained in the limit of zero temperature. Hagimásy *et al.* [25] calculated a more general formula of $I(\varphi,T)$ for finite temperature T and arbitrary junction length L. However, an analytic expression for the Josephson current cannot be obtained except for $T = 0$. Indeed, for vanishing temperature the expression by Hagimásy *et al.* correctly converges to that obtained by Titov and Beenakker. Instead, for $T \to T_c$ the nonsinusoidal supercurrent derived by Hagimásy *et al.* converges to a sinusoidal behavior, in both long and short junction regimes. In the short-junction limit, cf. Fig. 1(a) and Fig. 3(a) in Ref. [25], as long as $T \lesssim T_c/4$, the critical current and $I(\varphi,T)$ hardly change, so that Titov and Beenakker's formula remains valid [92]. This temperature threshold can be also deduced from the gap equation of the BCS theory; cf. Eq. (8) of Ref. [25]. Also for a short ballistic *vertical* SGS junction, Lee *et al.* [40] calculated the CΦR as a function of the temperature and transparency of the junction. This relation matches the CΦR found by Hagimásy *et al.* considering proper boundary conditions (cf. Eq. (1) of Ref. [40] and Eq. (7) of Ref. [25]).

The phase dynamics in graphene-based JJs, presented in this paper, is therefore strictly valid in a wide range of temperature values, and represents a good approximation for temperatures far from the critical value. For completeness, in the long-junction limit ($L \gg W$), the Josephson current reduces to

$$I(\varphi,T) = \frac{e\Delta}{\hbar}\tanh\left(\frac{\Delta}{2T}\right)e^{-\pi L/W}\sin\varphi = I_c(T)\sin\varphi, \tag{8}$$

showing the same φ dependence of conventional JJs (see Supplemental Material of Ref. [38]).

Lambert *et al.* [24], for an SGS junction, obtained from the expression of the current [Eq. (6)] the following washboard-like potential,

$$\tilde{U}(\varphi,t) = -E_{J0}\left\{-\frac{2}{1.33}\left\{2\sin\left(\frac{\varphi}{2}\right)\tanh^{-1}\left[\sin\left(\frac{\varphi}{2}\right)\right] + \ln\left[1-\sin^2\left(\frac{\varphi}{2}\right)\right]\right\} + i_b(t)\varphi\right\}, \tag{9}$$

and the expression of the plasma frequency

$$\tilde{\omega}_p = \sqrt{\frac{1}{m}\frac{d^2\tilde{U}}{d\varphi^2}\bigg|_{\varphi_{\min}}} = \frac{\omega_{p_0}}{\sqrt{1.33}}\sqrt{1-\sin\left(\frac{\varphi_{\min}}{2}\right)\tanh^{-1}\left[\sin\left(\frac{\varphi_{\min}}{2}\right)\right]}, \tag{10}$$

where $\varphi_{\min}$ is the value of the order parameter at the minimum of $\tilde{U}(\varphi,t)$, close to $\varphi = 0$.

The analytic knowledge of the potential allows us to well impose the initial condition and the thresholds for the escape time calculations. As well as the conventional $U(\varphi,t)$ [see Eq. (3)], the potential $\tilde{U}(\varphi,t)$ consists of a tilted sequence of wells. In the *superconductive state* the particle lies in a well, while in the *resistive state* it rolls down along the potential. When this happens, a nonzero mean voltage V across the junction appears, according to the *ac Josephson relation*, $\varphi_t = 2\pi V/\Phi_0$ [41,42]. Furthermore, depending on the damping parameter value, the *phase diffusion regime* [93,94], characterized by an escape process with a retrapping event in the first subsequent minimum, could be established. When $i_b(t) \geqslant 1$, that is, when the applied bias current exceeds the critical value, both potentials [Eqs. (3) and (9)] lose their "maxima and minima" structures and the particle tends to freely slip.

We analyze the response of the system to the simultaneous action of both dc and ac current sources. The bias current, composed of a constant term, i_0, representing its initial value, and an oscillating part whose frequency ω is normalized to ω_{p_0}, is therefore given by

$$i_b(t) = i_0 + A\sin(\omega t), \tag{11}$$

with maximum and minimum values (i_b^+ and i_b^-, respectively) given by

$$i_b^\pm = i_0 \pm A. \tag{12}$$

By choosing properly the values of i_0 and A, within a period it is possible to achieve values of $i_b(t)$ greater than 1. A direct comparison between the potentials for normal and graphene-based JJs is given in Fig. 2 for $i_0 = 0.0$ [panel (a)], 0.5 [panel (b)], and 0.9 [panel (c)]. Here it is worth noting that differences, though small, between the graphene and normal JJ curves are detectable. Figure 2 shows also the initial condition for the virtual phase particle, i.e., the phase difference between the

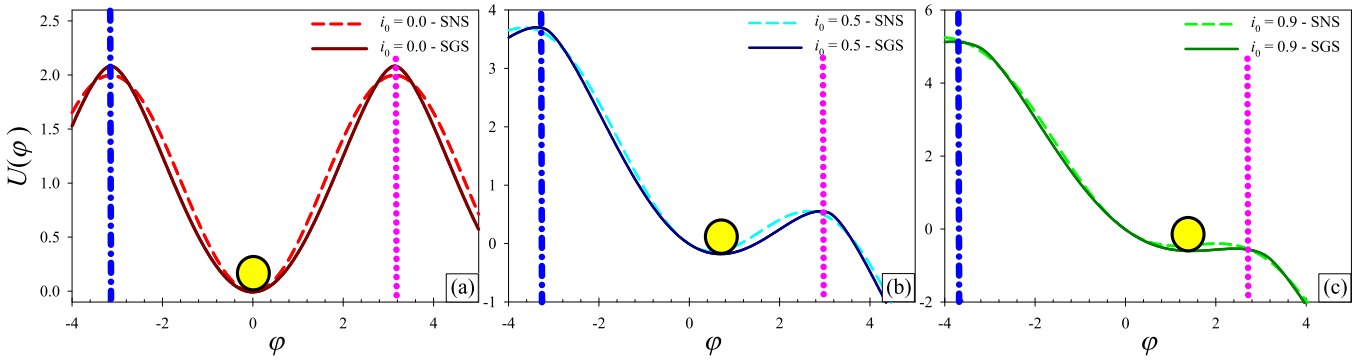

FIG. 2. (Color online) Washboard potential for SNS [see Eq. (3)] and SGS [see Eq. (9)] JJs (dashed and solid lines, respectively), for different values of the constant term of the bias current: $i_0 = 0.0$ (a), 0.5 (b), 0.9 (c). Also shown is the initial position (bottom of the potential well) of the "phase particle." Blue dotted-dashed and pink dotted lines indicate the left and right absorbing barriers, respectively.

wave functions of the two superconductors, which is located in the potential minimum. The system leaves the superconductive regime when the particle reaches one of the nearest maxima. Two absorbing barriers are therefore placed in these maxima, as highlighted in Fig. 2 (see dotted and dotted-dashed lines). Recording for each realization the escape times t^{esc}, that is, the time required to pass a barrier, for a large enough number N of realizations, the mean first passage time or *mean switching time* (MST) is defined as

$$\tau = \frac{1}{N}\sum_{i=1}^{N} t_i^{esc}. \tag{13}$$

The oscillating force acting on the system, $i_b(t)$, and stochastic fluctuations, $i_f(t)$, due to the environmental influence, drive the switching dynamics. Two different mechanisms can therefore cause overcoming of the potential barrier: the macroscopic quantum tunneling or the thermally activated passage. These processes are mainly triggered in two ranges of temperature so that, for vanishing values of the bias and damping, a threshold value exists, $T_{co} = \hbar\omega_{p_0}/2\pi k$, where k is the Boltzmann constant, called *crossover temperature*. In a damped system, when a polarization current is applied, this value is slightly reduced, becoming [95]

$$T_{co}^{\star} = \hbar\omega_R/2\pi k, \tag{14}$$

where

$$\omega_R = \omega_P\{\sqrt{1+\alpha^2} - \alpha\}, \tag{15}$$

and

$$\alpha = (2\omega_P R_N C)^{-1} \propto \beta_J. \tag{16}$$

For $T < T_{co}^{\star}$ the system undergoes a *quantum tunneling regime*. On the other hand, for $T > T_{co}^{\star}$, the system works in the *thermal activation regime*.

Here quantum effects are not taken into account. In this condition, when thermal fluctuations are neglected, the phase can remarkably change merely as the applied current approaches the critical value I_c (the system moves into a resistive regime). Conversely, considering noise effects, transitions between the potential wells can occur also applying a current much smaller than I_c. As already pointed out, the phase dynamics is affected by dissipative phenomena, responsible for dynamical peculiar behaviors of the system. In fact, the system can work both in overdamped (high viscosity $\beta_J \gg 1$) or underdamped (low viscosity $\beta_J \ll 1$) conditions. Table I shows a collection of a few experimental values for different graphene-based JJs, calculated or, whenever possible, directly acquired by several published works [12,13,36–39]. Blank cells indicate values not available. The values of the parameters $\beta_C = {\beta_J}^{-2}$ suggest that these systems often [36,38] work in underdamped conditions. Moreover, the comparison between the working temperature T and the crossover value $T_{co}^{\star}$ underlines the thermally activated switching behavior of these junctions [36–38].

The noise source. A comprehensive analysis of a real device must take account of environmental fluctuations. These, in fact, always affect the system by changing its dynamic regime. These environmental fluctuations produce, for example, unpredictable changes of current and temperature. Thus the deterministic RCSJ model must be modified by considering the presence of a stochastic current i_f [see Eq. (1)], which can be modeled by a Gaussian "white" noise source, as a first approximation. The stochastic nonnormalized current $I_f(\tilde{t})$ is therefore characterized by the well-known statistical properties of a Gaussian random process

$$\langle I_f(\tilde{t})\rangle = 0, \quad \langle I_f(\tilde{t})I_f(\tilde{t}+\tilde{\theta})\rangle = 2\frac{kT}{R_N}\delta(\tilde{\theta}), \tag{17}$$

where $\tilde{t}$ and $\tilde{\theta}$ are nonnormalized times, δ is the Dirac delta function, and T is the temperature. Using normalized units for current and time, the correlation function becomes

$$\langle i_f(t)i_f(t+\theta)\rangle = 2\gamma(T)\delta(\theta), \tag{18}$$

where the dimensionless amplitude $\gamma(T)$ is proportional to the temperature T. We note that the expression of $\gamma(T)$ depends on the approach used to analyze Eq. (1); specifically

$$\text{McCumber:} \quad \gamma^c(T) = \frac{kT}{R_N}\frac{\omega_c}{I_c^2} = \frac{2e}{\hbar}\frac{kT}{I_c} = \frac{kT}{E_J}, \tag{19a}$$

$$\text{Johnson:} \quad \gamma^p(T) = \frac{\omega_{p_0}}{\omega_c}\gamma^c(T). \tag{19b}$$

It is worth noting that the noise intensity can be also expressed as the ratio between the thermal and Josephson coupling energy [see Eq. (19a)]. Some γ^c values, calculated for several

experimental settings, are shown in Table I. More generally, the noise current $i_f(t)$ is the sum of thermal $i_{f_{th}}(t)$ and colored $i_{f_{co}}(t)$ Gaussian noise sources, that is, $i_f(t) = i_{f_{th}}(t) + i_{f_{co}}(t)$. To analyze in more detail the effect of the noise correlation time on the MST, we will consider fixed white thermal noise current with very low intensity by varying the parameters of the colored noise current to calculate the MST from Eq. (1). Specifically, the colored noise current $i_{f_{co}}(t)$ is described by the well-known Ornstein-Uhlenbeck (OU) process [96]

$$di_{f_{co}}(t) = -\frac{1}{\tau_c} i_{f_{co}}(t)dt + \frac{\sqrt{\gamma}}{\tau_c} dW(t), \tag{20}$$

where γ and τ_c are the intensity and correlation time of the noise source, respectively, and $W(t)$ is the Wiener process, characterized by the well-known statistical properties $\langle dW(t)\rangle = 0$ and $\langle dW(t)dW(t')\rangle = \delta(t-t')dt$.

The correlation function of the OU process is

$$\langle i_{f_{co}}(t) i_{f_{co}}(t')\rangle = \frac{\gamma}{2\tau_c} e^{-\frac{|t-t'|}{\tau_c}}, \tag{21}$$

and gives $\gamma\,\delta(t-t')$ in the limit $\tau_c \to 0$.

Computational details. The stochastic dynamics of the system is analyzed by integration of Eqs. (1) and (20) with a finite-difference method. Specifically, both stochastic differential equations are integrated within the Ito scheme. The time step is fixed at $\Delta t = 10^{-3}$ and the maximum time, for which equations are integrated, is $t_{max} = 100$. For our system, this t_{max} is a time large enough to catch every nonmonotonic behavior. A collection of first passage times is obtained iterating the procedure for a sufficiently large number of realizations $N = 10^4$. The initial condition to solve Eq. (1) is set at the bottom of a valley of the potential given in Eq. (9), close to $\varphi = 0$. During the oscillation of the potential the two absorbing barriers change their position, following the displacements of the neighboring maxima. The analysis is performed in the underdamped regime, setting $\beta_J = 0.1$ (corresponding to $\beta_C = 100$). Four different values of i_0, in the range $0 \leqslant i_0 < 1$, are used. The time periodical component of $i_b(t)$ oscillates with values of the frequency ω ranging within the interval [0.01,10]. In our analysis the intensity γ of the white noise source $i_f(t)$ [Eq. (18)] varies in the range $[10^{-4},10^2]$. For the analysis of MST in the presence of thermal white and colored noise sources, the intensity of the thermal noise current $i_{f_{th}}(t)$ is fixed at a value of 10^{-4}, and the intensity γ of the colored noise source $i_{f_{co}}(t)$ [Eq. (20)] varies in the range $[10^{-4},10^2]$, with the correlation time τ_c set at different values. As a consequence, this analysis is valid for JJs working at low temperatures.

III. THE ANALYSIS

The analysis is performed studying the behavior of the MST, τ, as a function of the noise intensity γ and frequency ω of the oscillating term in the bias current.

In Eq. (11) $i_0 = \{0.0,0.1,0.5,0.9\}$, corresponding to vanishing, small, intermediate, and high values, respectively, of the average slope of the washboard potential. The instantaneous slope of the potential, that is, the value of $i_b(t)$, is directly related to the height of the potential barriers, so that, increasing the value of $i_b(t)$, the right barrier's height decreases, becoming zero when $i_b(t) \geqslant 1$. The normalized amplitude of the oscillating term of the bias current is set at $A = 0.7$ in all numerical realizations.

The values of τ are presented in three-dimensional plots to highlight the simultaneous presence of different nonmonotonic effects. The values of γ are proportional, through Eqs. (19), to the temperature of the system, so that varying the noise intensity in the interval $\gamma = [10^{-4},10^2]$ corresponds to considering a wide range of temperatures. The noise amplitude values, calculated in different contexts and presented in Table I, fall within this range. The values of the frequency ω are chosen to investigate different regimes of alternate current: (i) quasidirect current ($\omega \ll 1$); (ii) high-frequency alternate current ($\omega \gg 1$); (iii) alternate current oscillating at frequencies close to the characteristic plasma frequency of the junction ($\omega \sim 1$). Because of the normalization factor of ω, the different values of ω_{p_0} in Table I give a quantitative estimation of the corresponding nonnormalized values of the driving frequency. The correlation time of the colored noise source takes the values $\tau_c = 0.0$ (i.e., white noise), 1.0,5,10.

It is worthwhile to note that for frequencies higher than the plasma frequency [see Eq. (10)], at low noise intensities, a trapping phenomenon occurs [59]. A threshold frequency ω_{thr} exists such that for $\omega > \omega_{thr}$ the *phase particle* is trapped within a region between two successive minima of the potential profile. Accordingly, the phase particle cannot move from the potential well to the next valley during one period of the driving current [see Eq. (11)]. As a consequence, the MST diverges in the limit $\gamma \to 0$. The value of the threshold frequency increases with increasing bias current and/or maximal current across the junction [52,59,97,98]. We have estimated the threshold values for three initial values of the bias current $i_0 = 0.1,0.5,0.9$. Specifically, we have $\omega_{thr}^{0.1} \simeq 1.04$, $\omega_{thr}^{0.5} \simeq 1.2$, and $\omega_{thr}^{0.9} \simeq 2.4$.

The results, shown in Fig. 3, were obtained using a white noise source, that is, setting $\tau_c = 0.0$, and for different values of the initial bias current (slope of the potential), i.e., $i_0 = 0.0$ [panel (a)], 0.1 [panel (b)], 0.5 [panel (c)], 0.9 [panel (d)]. In all panels of Fig. 3, the values of the other parameters are $A = 0.7$ and $\beta_J = 0.1$. First we note that a general lowering of τ values occurs with increasing i_0. This behavior is related to the modifications in the height of the barriers by changing the mean slope of the potential (see Fig. 2). The presence of two absorbing barriers allows us to consider both escape events of the phase particle to the left and right with respect to the initial state (minimum of the potential profile). Considering a highly tilted potential profile [panel (c) of Fig. 2], the particle rolls down preferably overcoming the potential barrier on the right. Conversely, with a small value of the initial bias current [panel (a) of Fig. 2], escape events may occur through the left potential barrier, and this gives rise to interesting phenomena. In particular, for $i_0 = 0.0$, the heights of the left and right barriers take on the same values within the first and second half of the oscillation period of the potential. Therefore, the particle can escape through the left or right barrier with equal probability.

In all panels of Fig. 3 a nonmonotonic behavior is evident, characterized by a minimum, which indicates the presence of the *resonant activation* (RA) phenomenon [98–109]. This effect is robust enough to be detected in a large range of γ values, even if it tends to be suppressed as the intensity

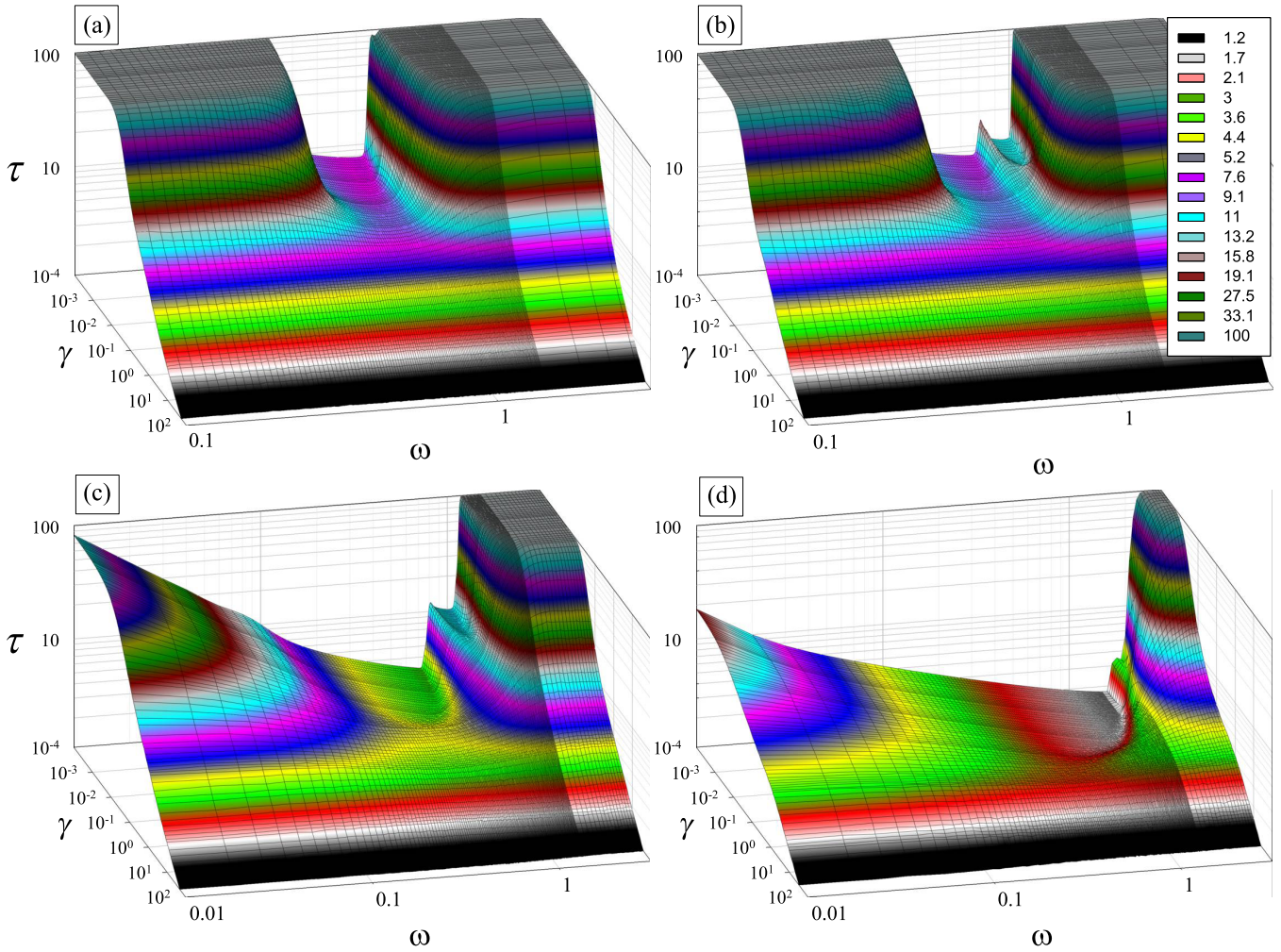

FIG. 3. (Color online) MST as a function of both ω and γ, for $\tau_c = 0.0$ and different initial values of the bias current: (a) $i_0 = 0.0$ (no slope), (b) $i_0 = 0.1$ (small slope), (c) $i_0 = 0.5$ (intermediate slope), (d) $i_0 = 0.9$ (high slope). In all panels the values of the other parameters are $A = 0.7$, $\beta_J = 0.1$. The legend in panel (b) refers to all pictures.

of thermal fluctuations increases. In other words, increasing γ, the minimum in the curves of MST vs ω becomes less pronounced. In particular, two different kinds of RA can be distinguished: (i) the *dynamic resonant activation* (DRA), which occurs as the external driving frequency is close to the natural characteristic frequency of the system, that is, the plasma frequency of the JJ [110–112]; (ii) the *stochastic resonant activation* (SRA), which occurs for driving frequency close to the inverse of the average escape time at the minimum, i.e., the mean escape time over the potential barrier in the lowest configuration [63,70,107].

The DRA is evident in the absence of a noise source ($\gamma = 0$) and in the quasideterministic regime ($\gamma \ll 1$), when the dynamics depends mainly on the profile of the washboard potential. Increasing the noise intensity, the SRA tends to become predominant and hides every DRA effect. Figure 4(a) shows the behavior of the MST vs ω, with the noise intensity fixed at such a small value that the DRA effect can be clearly observed and studied as a function of the initial bias current i_0. For such a low noise intensity we can say that the SRA is hidden.

In more detail, in Fig. 4(a) are shown the results obtained for graphene-based SGS (solid lines) and normal SNS (dotted lines) JJs for $\gamma = 10^{-4}$. The values of τ, in correspondence to the DRA minima, are almost independent of the type of the junction, SNS or SGS. Moreover, the values of DRA minima, for an SNS JJ, are shifted towards higher frequencies with respect to those obtained for an SGS JJ. Furthermore, for small bias current i_0, the DRA minima for an SNS JJ are slightly narrower than those calculated for an SGS JJ.

The DRA effect occurs when the frequency ω of the oscillating washboard potential matches a characteristic frequency of the system. It is worth noting that, due to the time dependence of the bias current $i_b(t)$, a JJ is characterized by a continuous spectrum of values of ω_P according to Eqs. (4) and (10). In Fig. 4(a), for $i_0 = 0.0$ and an SGS junction, a single-minimum of DRA at $\omega_{dRA}^{0.0} \simeq 0.81$ is evident. The *phase particle* feels an effective plasma frequency which can be approximated by the time average of the plasma frequency $\overline{\tilde{\omega}_p}$ in a period of the driving current. This averaged plasma frequency is $\overline{\tilde{\omega}_p} \simeq 0.81$.

Slightly increasing the initial bias current, the DRA effect becomes more "structured". Indeed, for $i_0 = 0.1$ the same effect occurs with the presence of two minima located at

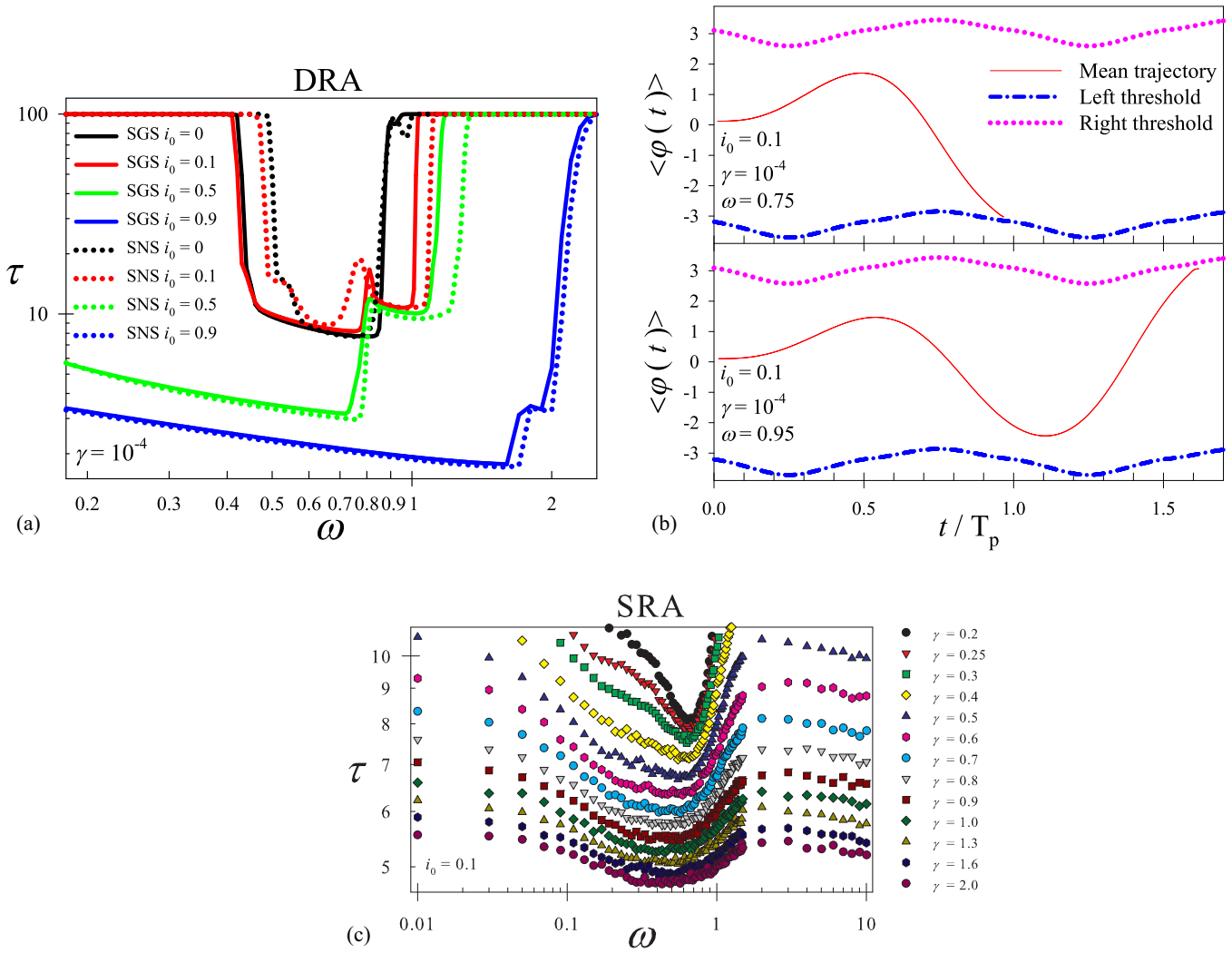

FIG. 4. (Color online) (a) MST as a function of the driving frequency ω, for $\gamma = 10^{-4}$, and different initial values of the bias current, namely $i_0 = \{0.0,0.1,0.5,0.9\}$. Solid and dotted lines represent results for SGS and SNS junctions, respectively. The dynamical resonant activation phenomenon is clearly evident. (b) Ensemble average trajectories of the *phase particle* for two values of the driving frequency, that is, $\omega_{dRA}^{0.1} \simeq 0.75$ and 0.95, corresponding to the two minima of DRA observed at $i_0 = 0.1$. Blue dotted-dashed and pink dotted lines indicate the left and right absorbing barriers, respectively. (c) MST as a function of the driving frequency ω, for $i_0 = 0.1$ and different values of noise intensity γ ranging from 0.2 to 2. The stochastic resonant activation phenomenon is clearly evident. In all panels the values of the other parameters are $\tau_c = 0.0$, $A = 0.7$, $\beta_J = 0.1$.

$\omega_{dRA}^{0.1} \simeq \{0.75,0.95\}$ [see Fig. 4(a)]. The presence of these two minima is related to as many *escape resonance phenomena*. Nonvanishing values of the initial bias current ($i_0 \neq 0$) introduce an asymmetry; e.g., with $i_0 = 0.1$ the highest and lowest slope are respectively $|i_b^+| = 0.8$ and $|i_b^-| = 0.6$. As a consequence, the time average plasma frequencies in the first half and in the second half period of the driving current are different. Specifically we have in the first half period $\overline{\tilde{\omega}_p^a} \simeq 0.78$ and in the second half period $\overline{\tilde{\omega}_p^b} \simeq 0.83$. These plasma frequency values are an approximation of the effective plasma frequencies felt from the phase particle. In fact, they are obtained by Eqs. (4) and (10), which are valid in the harmonic approximation of the potential profile around the minima [49]. From the behavior of the average trajectories shown in Fig. 4(b), we see that the resonant escape process occurs for low driving frequency at $t \simeq T_p$ [see top panel of Fig. 4(b)], and for high driving frequency at $t \simeq 1.6T_p$ [see bottom panel of Fig. 4(b)]. Due to the dynamics of the resonance phenomenon between the effective plasma frequency and the external driving frequency, the first escape process (which occurs at low frequency) is resonant with the effective plasma frequency felt by the particle in the first half period of the driving current [see top panel of Fig. 4(b)]. This effective plasma frequency is approximated by the time average plasma frequency $\overline{\tilde{\omega}_p^a} \simeq 0.78$. The second escape process (which occurs at high frequency) is resonant with the effective plasma frequency felt by the particle in the second half period of the driving current [see bottom panel of Fig. 4(b)]. This effective plasma frequency is approximated by the time average plasma frequency $\overline{\tilde{\omega}_p^b} \simeq 0.83$.

In Fig. 4(c), the curves of MST as a function of the driving frequency ω, for $i_0 = 0.1$ and different values of noise intensity γ ranging from 0.2 to 2, are shown. The SRA phenomenon is clearly evident. In fact, it occurs for a driving frequency close

to the inverse of the average escape time over the potential barrier in the lowest configuration.

Trapping phenomena occur for $\omega \gtrsim 1$. However, these trapping phenomena tend to disappear for high values of the noise intensity.

Since $A = 0.7$, for $i_0 = \{0.5,0.9\}$ the potential is tilted enough to lose in the lowest configurations the characteristic "maxima and minima" structure. If $i_0 = 0.5$ the double-minimum dynamic RA is still present around the frequencies $\omega_{dRA}^{0.5} \simeq \{0.72,1.02\}$ [see Fig. 4(a)]. The MST value $\tau \simeq 3.2$ in correspondence with the first RA minimum obtained for $i_0 = 0.5$ is smaller than that obtained for $i_0 = 0.1$, that is $\tau \simeq 8.3$. This is due to the fact that the slope $i_0 = 0.5$ is able to induce a rightward escape event already after a quarter of an oscillation period T_p of the potential [indeed $\tau(\omega \equiv \omega_{dRA}^{0.5} = 0.72) \sim T_p/4$], whereas for $i_0 = 0.1$ the particle needs one complete oscillation of the potential to escape, and $\tau(\omega \equiv \omega_{dRA}^{0.1} = 0.75) \sim T_p$ [see Fig. 4(a)]. On the other hand, the values of τ in the second RA valley for $i_0 = 0.1$ and $i_0 = 0.5$ are almost equal, since the particle needs more than one complete oscillation (for both slopes $\tau \simeq 1.6T_p$) to escape from the right potential barrier. In fact, from the analysis of the average trajectory for $i_0 = 0.5$, the escape process for high driving frequency is resonant with the effective plasma frequency felt by the particle in the second half period of the driving frequency, as in the case of $i_0 = 0.1$ [see bottom panel of Fig. 4(b)]. For $i_0 = 0.5$, this effective plasma frequency is approximated by the time average plasma frequency, in the second half period, $\overline{\tilde{\omega}_p^b} \simeq 0.85$.

Setting $i_0 = 0.9$, corresponding to a highly tilted potential, the DRA effect is just hinted and only the minimum around $\omega_{dRA}^{0.9} \simeq 1.6$ is evident [see Fig. 4(a)].

Trapping phenomena at high frequencies are still present. Specifically, these appear for frequencies greater than the threshold values $\omega_{thr}^{0.5} \simeq 1.2$ and $\omega_{thr}^{0.9} \simeq 2.4$ [see Fig. 4(a)]. We point out that, increasing the value of the bias current, the right potential barrier decreases. As a consequence, trapping phenomena can occur only if the potential oscillates at high frequencies. This remark, together with the statement that the parabolic approximation (linearization of the potential at the bottom of the well), used to calculate the plasma frequency according to Eqs. (4) and (10), fails for highly tilted potentials, explains why the threshold values $\omega_{thr}^{0.5}$ and $\omega_{thr}^{0.9}$ are significantly higher than 1 [see Fig. 4(a)].

We focus now on the influence of the damping on the DRA phenomenon. We study the effects of a slight increase of the damping parameter β_J on the double-minimum structure of the DRA effect, which occurs in the behavior of the MST as a function of the driving frequency ω, setting $i_0 = 0.1$ and $\gamma = 10^{-4}$. This is shown in Fig. 5 for $\beta_J \in [0,0.45]$. We observe that by increasing the damping parameter β_J the τ values in the bottom of the wells tend to increase, so much so that for $\beta_J \gtrsim 0.45$ the DRA effect for $\gamma = 10^{-4}$ vanishes. The double-minimum structure, which is evident for $\beta_J \in [0,0.16[$, disappears and a large "single-minimum" DRA effect emerges for $\beta_J \in [0.16,0.45[$. In fact, increasing the viscosity of the system the mobility of the phase particle reduces, so that the particle is not able to reach the left barrier before the oscillation of the driving pushes it again towards the right. Accordingly, the DRA effect occurs exclusively throughout the right potential barrier. The height of the maximum of τ

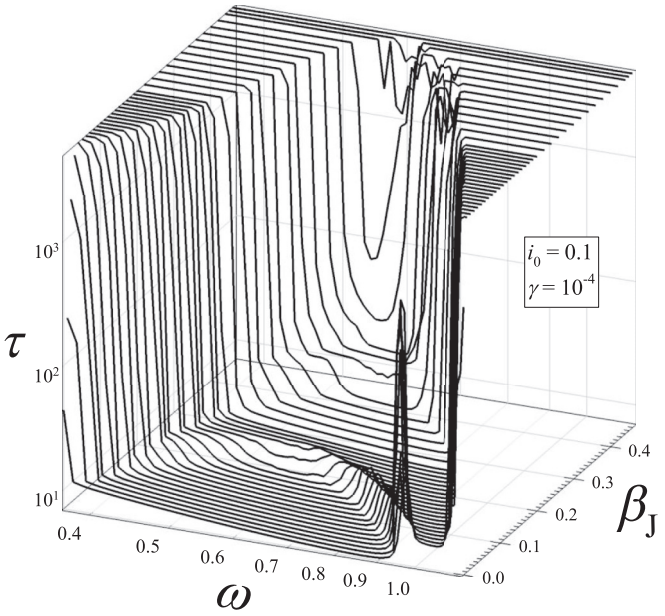

FIG. 5. MST as a function of the driving frequency ω and the damping parameter β_J, for $\gamma = 10^{-4}$, $\tau_c = 0.0$, $i_0 = 0.1$, and $A = 0.7$.

between the DRA minima tends to reduce, up to vanishing, for $\beta_J \gtrsim 0.16$. This peak of τ, for low damping, occurs in correspondence with out-of-resonance escape processes between the left and right DRA minima (see Fig. 5). The corresponding dynamics is characterized by a longer residence time of the phase particle within the initial potential well.

Increasing the damping, the probability that these trajectories with a longer lifetime occur tends to decrease. Indeed, due to the reduced mobility, the phase particle will escape in average at the first resonant escape process available during its trajectory. For $\beta_J \gtrsim 0.45$ the particle is slowed down so that also the right barrier cannot be reached before the driving oscillations push again the particle to the left. Therefore the particle tends to remain confined within the potential well throughout the simulation time.

In all panels of Fig. 3 we note the presence of another noise-induced effect, known as *noise-enhanced stability* (NES) [59,97,98,108,109,113–126]. Indeed the curves of τ vs γ are characterized by a nonmonotonic behavior with the presence of a maximum. This nonmonotonic behavior is different from that expected from the Kramers theory and its extensions [127–129]. The enhancement of stability present in the curves of Fig. 3, first noted by Hirsch *et al.* [130], has been observed in different physical and biological systems, and belongs to a highly topical interdisciplinary research field, ranging from condensed matter physics to molecular biology and cancer growth dynamics [119,131–135].

Specifically, the behaviors of τ vs γ show the presence of NES for any frequency within an interval around the different values of the frequencies $\omega_{dRA}^{i_0}$, as found in previous theoretical investigations of the NES phenomenon [98,97]. In particular, for $i_0 = 0.0$ this effect occurs for $\omega_{NES} \in [0.43,0.87]$. For each value $i_0 = 0.1,0.5$ of the bias current, there are two $\omega_{dRA}^{i_0}$ frequencies and, correspondingly, two different ranges of frequencies giving rise to NES effects. In detail: $\omega_{NES}^{(1)} \in$

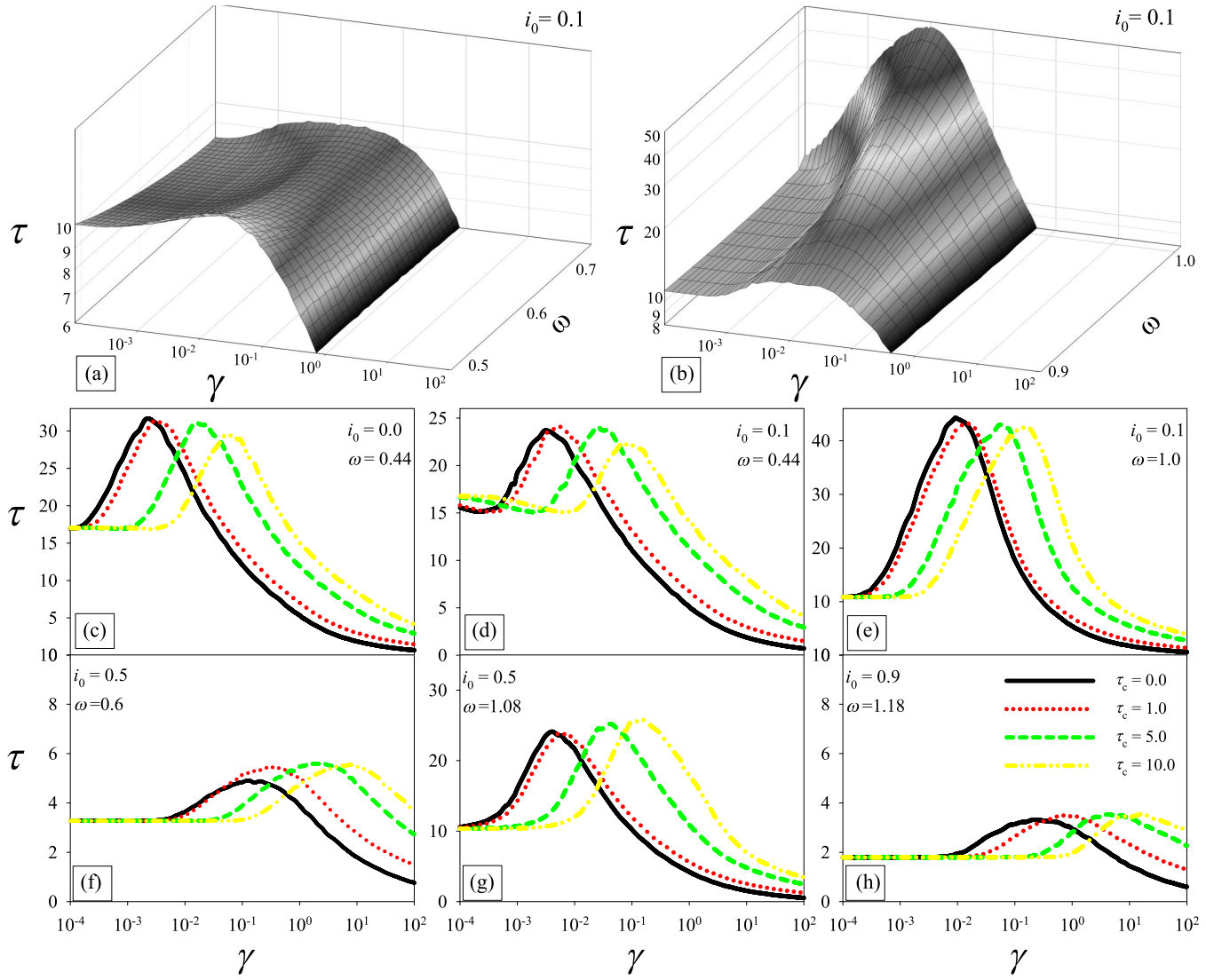

FIG. 6. (Color online) MST as a function of γ, for different values of ω, i_0, and τ_c. Specifically, (a) $i_0 = 0.1$, $\omega \in [0.49,0.77]$ and $\tau_c = 0.0$; (b) $i_0 = 0.1$, $\omega \in [0.9,1.02]$ and $\tau_c = 0.0$; (c) $i_0 = 0$, $\omega = 0.44$; (d) $i_0 = 0.1$, $\omega = 0.44$; (e) $i_0 = 0.1$, $\omega = 1.0$; (f) $i_0 = 0.5$, $\omega = 0.6$; (g) $i_0 = 0.5$, $\omega = 1.08$; (h) $i_0 = 0.9$, $\omega = 1.18$. The values of the other parameters are $A = 0.7$, $\beta_J = 0.1$. The legend in panel (h) refers to all pictures except to panels (a) and (b).

$[0.42,0.78]$ and $\omega_{NES}^{(2)} \in [0.84,1.02]$ for $i_0 = 0.1$ [see panels (a) and (b) of Fig. 6, respectively], and $\omega_{NES}^{(1)} \in [0.24,0.77]$ and $\omega_{NES}^{(2)} \in [0.97,1.14]$ for $i_0 = 0.5$.

Using a highly tilted potential, i.e., $i_0 = 0.9$, there is only one large RA minimum and only one range of frequencies $\omega_{NES} \in [0.4,2.4]$ for which the NES phenomenon is found. According to this analysis, the curves of Fig. 6, obtained for different values of the noise correlation time ($\tau_c = 0.0,1.0,5,10$), show the presence of NES for values of ω chosen in the intervals given above. In all curves, as τ_c increases, the maxima are shifted towards higher values of the noise intensity. Moreover, the MST values around the NES maxima tend to slightly reduce for low slopes (small values of i_0) of the oscillating potential [panels (c), (d), and (e) of Fig. 6] and to increase for high slopes [panels (f), (g), and (h) of Fig. 6].

These features, i.e., the shift towards higher noise intensities and modification in the maxima of MST for increasing values of τ_c, are present also in conventional JJs [53,58].

The curves of τ vs γ in Fig. 7, where $i_0 = 0.0$, $\omega = 0.75$, and $\beta_J = 0.1$, show that for an SNS JJ with respect to an SGS junction, (i) the NES maxima are broader; (ii) the phase particle remains confined in the potential well for longer time, i.e., the τ values are slightly higher; (iii) the NES effect appears for lower noise intensities. Conversely, the behavior of normal and graphene JJs is the same for larger values of the noise intensity γ, since the details of the specific potential profile become irrelevant due to the strength of random fluctuations.

IV. PROBABILITY DENSITY FUNCTIONS

To deeply understand the stochastic process of escape from the metastable state, we extend the theoretical analysis, presenting and discussing the probability density functions (PDFs) of the switching times, $P(t)$. The distributions of the escape times have been investigated in many unstable physical systems, in which noise enhancement stability [114,136]

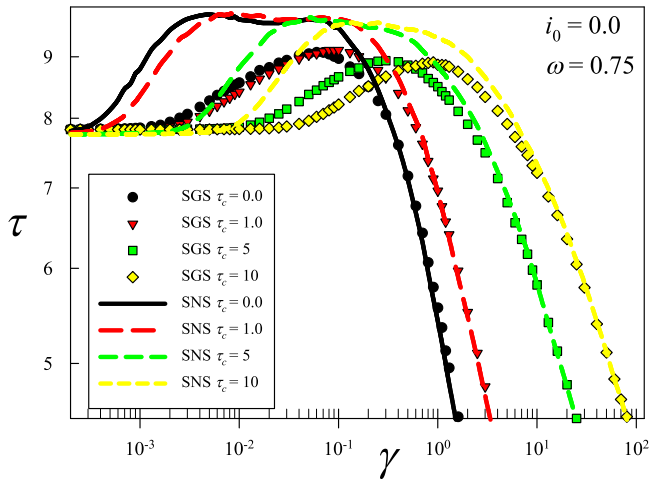

FIG. 7. (Color online) MST as a function of γ, for $\omega = 0.75$, $i_0 = 0.0$, $A = 0.7$, $\beta_J = 0.1$ and different values the noise correlation time: $\tau_c = 0.0, 1.0, 5, 10$. Symbols and lines represent results for SGS and SNS junctions, respectively.

and resonant activation [100,101] phenomena have been observed. The analysis of the PDF supports investigations in many out-of-equilibrium frameworks, such as financial markets [137–139], polymer dynamics [140,141], and several biological systems [142].

The parameters of the system and noise source are set in such a way to put in evidence nonmonotonic effects in the MST behavior. Every PDF is constructed performing $N = 10^7$ numerical realizations (experiments), and the area under each curve is normalized to unit. Whenever possible, the escape time t is normalized to the driving period T_p of the washboard potential. This allows us to compare the passage times with the different slopes taken on by the potential during its oscillatory motion. We use log plots in Figs. 8 and 9 to appreciate also the lower peaks of the PDFs.

Panels (a), (b), (c), and (d) of Fig. 8 show $P(t)$ for different initial values of the bias current $i_0 = 0, 0.1, 0.5, 0.9$. These results allow us to analyze the switching dynamics in correspondence with interesting points of τ vs ω curves for low noise intensity $\gamma = 10^{-4}$ [see solid lines in Fig. 4(a) and in the t-ω planes of Fig. 8]. Setting the driving frequency to the value taken at the bottom of the RA minima, that is, $\omega \equiv \omega_{dRA}^{i_0}$, the resonance-like dynamics results in single-peak PDFs, centered around the MST. Correspondingly, we observe that, for $\omega \equiv \omega_{dRA}^{i_0}$, the phase particle tends to follow almost the same trajectory in each experiment to escape from the initial metastable state. Panel (e) of Fig. 8 shows the PDF of the normalized escape time t/T_p, calculated setting $\omega = \omega_{dRA}^{0.1} = 0.75, 0.95$. As already pointed out, setting $\omega = 0.75$, which is the frequency corresponding to the first dynamic RA minimum, the particle tends to escape mainly through the left barrier, in average after almost one oscillation of the washboard potential [see top panel of Fig. 4(b)]. Conversely, setting $\omega = 0.95$, which is in correspondence to the second dynamic RA minimum, mostly right-side escapes occur, on average, when $t \simeq 1.6 T_p$ [see bottom panel of Fig. 4(b)]. These peaks show asymmetry and exponential tails, as previously found for a cubic potential with a metastable state in experimental [100] and theoretical [101] investigations. The asymmetry is more pronounced in low-frequency data, because the time the washboard potential spends in the configurations favorable to the crossing of the barrier becomes longer by reducing the oscillation frequency, and this results in a spread of the

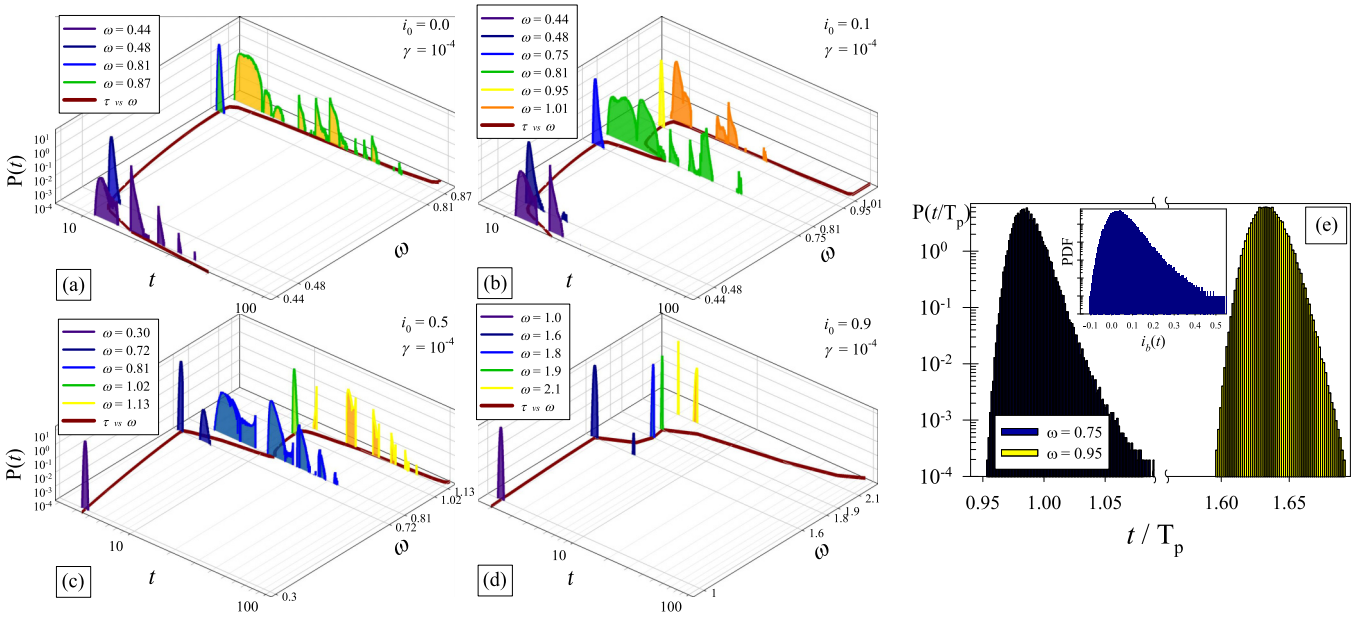

FIG. 8. (Color online) Panels (a), (b), (c), and (d): PDFs as a function of the time t, varying ω. Every picture is obtained fixing $\gamma = 10^{-4}$, $\tau_c = 0$, $A = 0.7$, and $i_0 =$ (a) 0.0, (b) 0.1, (c) 0.5, (d) 0.9. The MST τ vs ω curves, corresponding to the dynamic RA effect [see solid lines in Fig. 4(a)], are also shown. The PDF and t axes are logarithmic. Panel (e): Semilog plot of the PDFs as a function of the time t, normalized to the driving period T_p, setting $\gamma = 10^{-4}$, $\tau_c = 0$, $A = 0.7$, $i_0 = 0.1$, and $\omega = \omega_{dRA}^{0.1} = 0.75, 0.95$. The inset shows the PDF for $\omega = 0.75$ of the bias currents $i_b(t)$ corresponding to escape or switching events of panel (e).

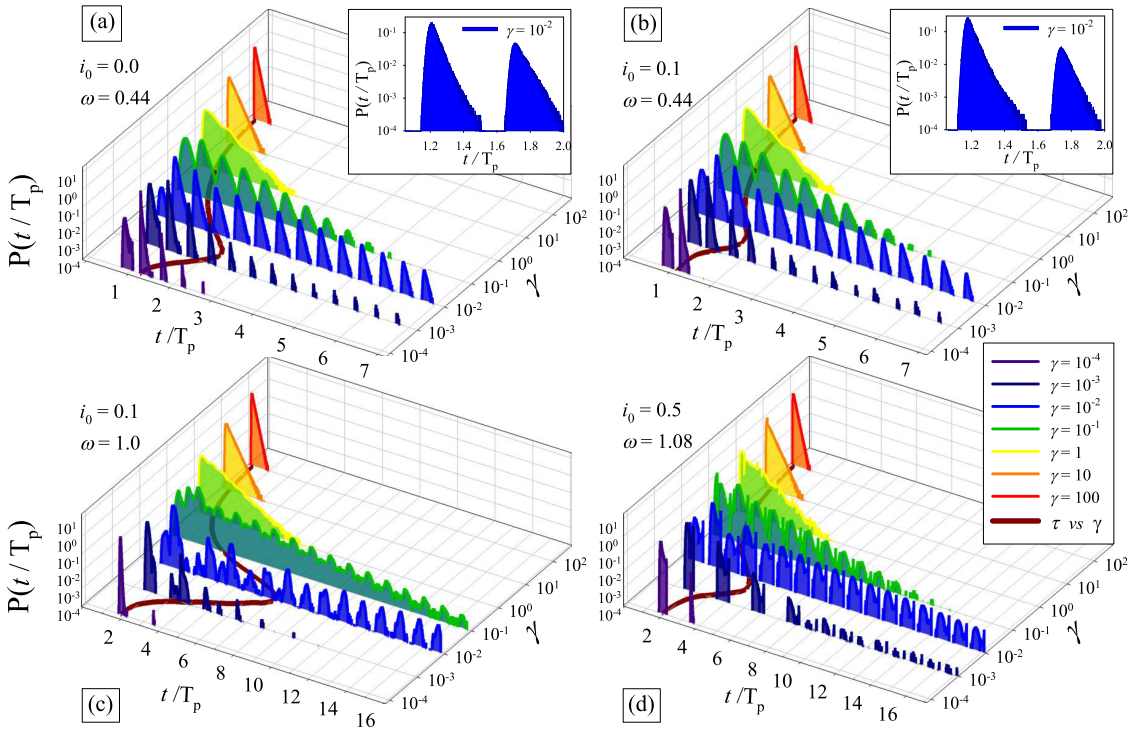

FIG. 9. (Color online) PDF as a function of the time t, normalized to the driving period T_p, varying γ. Every picture is obtained fixing $\tau_c = 0$, $A = 0.7$, and the values of i_0 and ω. In detail, in each panel (a) $i_0 = 0$, $\omega = 0.44$, (b) $i_0 = 0.1$, $\omega = 0.44$, (c) $i_0 = 0.5$, $\omega = 1.08$, and (d) $i_0 = 0.9$, $\omega = 1.18$. Every picture shows also the MST versus γ curve corresponding to the NES effect (see solid lines in Fig. 6), obtained using the same values for the other parameters. The insets in panels (a) and (b) show the detail of the peaks contained in one period of oscillation of the potential for $\gamma = 10^{-2}$. The PDF and γ axes are logarithmic. The legend refers to all panels.

escape trajectories. In other words, at low frequency, the escape processes tend to spread in time.

The inset in Fig. 8(e) shows, for $\omega = 0.75$, the PDF of the bias currents $i_b(t)$ corresponding to the escape events of panel (e). This PDF can be compared with the experimental thermally activated switching current distribution $P(I_c)$ in SGS junctions (cf. Fig. 1(c) of Ref. [46] and Fig. 2 of Ref. [38]). The shapes of these PDFs are similar, unless there is a reflection about the y axes in our PDF with respect to $P(I_c)$. The reflection occurs because the PDF for $\omega = 0.75$ represents leftward switching events [see top panel of Fig. 4(b)]. For these escape dynamics, as the bias current increases, the height of the potential barrier to be overcome by the particle increases, contrary to what occurs for the measurements of the $P(I_c)$ distributions. All the PDFs for frequencies within the dynamic RA minima are still formed by single peaks, whose width increases as they move far from the condition $\omega = \omega_{dRA}^{i_0}$ [see panels (a) and (b) of Fig. 8]. Sufficiently far from the dynamic RA frequencies, specifically when the τ values tend to grow, the PDFs are multipeaked, due to the periodical successive escape events.

The probability distributions associated with the average escape times shown in panels (c), (d), (e), and (g) of Fig. 6 for $\tau_c = 0$ (solid lines) are exhibited in panels (a), (b), (c), and (d) of Fig. 9, respectively. In detail, the values of the initial bias and driving frequency are $i_0 = 0$, $\omega = 0.44$ [panel (a)], $i_0 = 0.1$, $\omega = 0.44$ [panel (b)], $i_0 = 0.1$, $\omega = 1.0$ [panel (c)], $i_0 = 0.5$, $\omega = 1.08$ [panel (d)] and the normalized time t/T_p is used. These frequencies are within the dynamic RA minima and are chosen to maximize the NES effects. The PDFs shown in Fig. 9 give a better insight into the NES phenomenon. For this reason the solid curves of Fig. 6 are presented again in the t-ω plane of Fig. 9. When considering a Brownian particle in the presence of a metastable fluctuating potential with a strong driving force or current, the NES effect is always obtained, regardless of the initial position of the particle. The dynamical regime is characterized by the absence of the potential barrier for some short time interval; that is, the system in a deterministic regime is overall unstable [114]. After this time interval the Brownian particle, because of the interplay between the noise and the time-dependent driving force, can return into the potential well, and the mean lifetime of the metastable state increases with the noise intensity in comparison with the dynamical lifetime [97,98,114]. The presence of noise slows down the motion of deterministically overall unstable states in an appropriate range of potential parameters, contrary to what one might have expected [98,114,115,117,119]. Accordingly, in correspondence to the NES maxima, the PDFs are composed by long regular sequences of equidistant sharp peaks with exponentially decreasing amplitude. Multipeaked distributions of escape times with exponentially decaying envelopes characterize both experimental [114,143] and theoretical investigations [114,136,144]. It is worthwhile to note that for escape processes from metastable states the shape of each peak of the multipeak PDF is asymmetric [97], while it is symmetric for escapes from symmetric double-well potential profiles [144].

For small initial potential slopes [see panels (a) and (b) of Fig. 9] the PDFs are distributions of a series of two distinct peaks per driving period T_p, but an asymmetry with "tails"

in the shape of the peaks is observable. The distribution of the peaks is consistent with the study of the dynamics of a particle in a symmetric double-well potential in the presence of an additional sinusoidal driving [143,144]. In particular, in Refs. [143,144] the MST distributions for periodically driven systems at small driving frequencies, smaller than the noise-induced hopping rate, are discussed. The distribution of the escape times from the left potential well for $A \gg D$, where A and D are the sinusoidal driving amplitude and the noise intensity, respectively, is

$$P_{\frac{A}{D}\gg 1} \approx e^{\left[-\frac{A}{D}\cos(\omega t)\right]} \exp\left\{-\frac{r_0}{\omega}\sqrt{\frac{\pi D}{2A}}e^{\frac{A}{D}} \times \left[2n+1+\mathrm{erf}\left(\sqrt{\frac{A}{2D}}(\omega\bar{t}-\pi)\right)\right]\right\}. \quad (22)$$

Here, ω is the driving frequency, $\omega\bar{t} = \mathrm{mod}(\omega t, 2\pi)$, erf denotes the error function, and r_0 is the unperturbed Kramers rate [127],

$$r_0 = \pi^{-1}\sqrt{|U''(\varphi_{\mathrm{Max}})|U''(\varphi_{\mathrm{min}})}\exp\left(-\frac{\Delta U}{D}\right), \quad (23)$$

where $U''(\varphi_{\mathrm{min}})$ and $U''(\varphi_{\mathrm{Max}})$ are, respectively, the second derivatives in the minimum and the successive maximum of the potential, and ΔU is the barrier height, measured with respect to these two points of the potential.

In the opposite limit $A \ll D$, the escape time distribution is described by an exponential decay with a weak modulation

$$P_{\frac{A}{D}\ll 1} \propto r_0 e^{-r_0 t}. \quad (24)$$

Equation (22) is a multipeaked curve with peaks located, according to the factor $\exp\{-A/D\cos(\omega t)\}$, at odd multiples of the half driving period T_p and with an exponential envelope [129]. The second peak corresponds to the event that the system has not escaped during the first period, but has escaped during the successive period. The other peaks correspond to successive escapes.

In the PDFs obtained for low noise intensities, $\gamma \in [10^{-4}, 10^{-1}]$ [see panels (a) and (b) of Fig. 9], the series of peaks are formed by two distinct peaks per driving period, as it is clearly shown in the inset for $\gamma = 10^{-2}$. Differently from the escape processes occurring in the double-well analysis, the escape events from a washboard well can occur indeed across the left or right barrier, resulting in the two peaks per period. Specifically, the peaks placed in correspondence to the odd (even) multiples of the half driving period represent escape events through the right (left) potential barrier. The shape of the tails of these peaks is exponential, accordingly to the shape of the PDF of the escape times from a metastable state found analyzing the NES phenomenon [97]. Moreover, the exponential tail is also observed as a peculiarity of the PDF in the RA effect [101].

Increasing the noise intensity, $\gamma = 1$, 10, 100, the peaks tend to become lower and broader, up to merging into a larger distribution. Panels (c) and (d) of Fig. 9 refer to $i_0 = 0.1$ and 0.5, respectively, but the driving frequency is high enough ($\omega \geqslant 1$) to trap for long times the particle inside the initial well, generating interesting peak structures. Each period contains again two peaks with two particular shapes: the first one, a little bit narrower, appearing at times odd multiples of $T_p/2$, due to the rightward escapes for highly tilted potential; the second one, strongly asymmetric, appearing at times even multiples of $T_p/2$.

The peaks for high noise intensities, that is $\gamma = 10$ and $\gamma = 100$, are independent of the potential characteristics and extend approximately up to $t \simeq 11.5$ and $t \simeq 5.3$, respectively, regardless the oscillation frequency and the mean slope of the potential.

V. CONCLUSIONS

We analyzed the influence of thermal fluctuations on the behavior of a ballistic graphene-based Josephson junction (JJ) in the short-junction regime. In particular, we investigate how random fluctuations affect the lifetime of the superconductive state in an underdamped current-biased JJ. The analysis was performed within the framework of the resistively and capacitively shunted junction (RCSJ) model, using a proper nonsinusoidal current-phase relation, characteristic of a JJ made by a graphene layer partially covered by the superconducting electrodes. Specifically we investigated the mean switching time (MST) of the phase particle, i.e., the phase difference across the junction, initially placed in a minimum of the tilted washboard-like potential. In particular, we studied the MST as a function of different parameters of the system and external perturbations, i.e., Gaussianly distributed random fluctuations and periodical driving signal. We found nonmonotonic behavior of the lifetime τ of the superconductive state as a function of the noise intensity γ and the driving frequency ω, for different initial values i_0 of the bias current. In particular, we found that suitable values of γ determine maximum escape times, while minima are observed for certain values of the driving frequency. These results indicate the presence of noise-induced phenomena, such as *noise-enhanced stability* (NES) and *resonant activation* (RA) with different features, strongly depending on the initial value of the bias current. In more detail, in some ranges of the parameter values the behavior of MST indicates the presence of *dynamic* and *stochastic* RA, including a multiple-minimum RA effect in the low-noise intensity regime.

Finally, when the white noise source is replaced by a colored noise source with different values of the correlation time τ_c, we find modifications in the MST behavior. In detail, in the τ vs γ curves, when increasing τ_c, a shift towards higher noise intensities and changes in the NES maxima are observed.

The study is completed by the probability density function (PDF) analysis of the escape times, to relate the MST behavior with the trajectories followed by the phase particle to escape from the metastable state. For frequencies within the dynamic RA minima, the PDFs are formed by single peaks. These peaks show asymmetry and exponential tails. In correspondence to the NES maxima, the PDFs obtained for low noise intensities are composed of long regular sequences of two peaks per driving period, with exponentially decaying envelopes. The shape of these peaks depends on the features of the potential, such as the mean slope and the oscillation frequency. The presence of two peaks per period is consistent with the physical picture

that the crossing of the potential barrier takes place most likely in the "left" and "right" down positions of the potential.

In conclusion, this work is well placed in the framework of nonequilibrium statistical mechanics, due to the presence of a rich transient dynamics, observed in an emerging material, such as graphene, with unique electrical properties. In fact, our study provides information on the role played by random (both thermal and correlated) fluctuations in the switching dynamics from the superconductive state to the resistive one of a graphene-based JJ. The results obtained can help to better understand the role of fluctuations in the electrodynamics of new-generation graphene-based superconductive devices, such as Josephson junctions, Josephson sensors, dc SQUIDs, JJ detectors, and gate-tunable phase qubits, contributing to improving their performances.

ACKNOWLEDGMENTS

The authors acknowledge the financial support of the Ministry of Education, University, and Research of the Italian Government (MIUR) through Grant No. PON02_00355_3391233, "Tecnologie per l'ENERGia e l'Efficienza energETICa - ENERGETIC". The authors also wish to thank Dr. I. Hagymási and Dr. A. Carollo for fruitful discussions and useful suggestions.

[1] K. S. Novoselov, A. K. Geim, S. V. Morozov, D. Jiang, Y. Zhang, S. V. Dubonos, I. V. Grigorieva, and A. A. Firsov, Electric field effect in atomically thin carbon films, Science **306**, 666 (2004).

[2] A. H. Castro Neto, F. Guinea, N. M. R. Peres, K. S. Novoselov, and A. K. Geim, The electronic properties of graphene, Rev. Mod. Phys. **81**, 109 (2009).

[3] C. W. J. Beenakker, Specular Andreev Reflection in Graphene, Phys. Rev. Lett. **97**, 067007 (2006).

[4] M. Titov, A. Ossipov, and C. W. J. Beenakker, Excitation gap of a graphene channel with superconducting boundaries, Phys. Rev. B **75**, 045417 (2007).

[5] M. Maiti and K. Sengupta, Josephson effect in graphene superconductor/barrier/superconductor junctions: Oscillatory behavior of the josephson current, Phys. Rev. B **76**, 054513 (2007).

[6] B. Uchoa and A. H. Castro Neto, Superconducting States of Pure and Doped Graphene, Phys. Rev. Lett. **98**, 146801 (2007).

[7] A. Fedorov, N. Verbitskiy, D. Haberer, C. Struzzi, L. Petaccia, D. Usachov, O. Vilkov, D. Vyalikh, J. Fink, M. Knupfer, B. Büchner, and A. Grüneis, Observation of a universal donor-dependent vibrational mode in graphene, Nat. Commun. **5**, 3257 (2014).

[8] C. Girit, V. Bouchiat, O. Naaman, Y. Zhang, M. Crommie, A. Zettl, and I. Siddiqi, Tunable graphene dc superconducting quantum interference device, Nano Lett. **9**, 198 (2008).

[9] Ç. Girit, V. Bouchiat, O. Naaman, Y. Zhang, M. F. Crommie, A. Zettl, and I. Siddiqi, Current–phase relation in graphene and application to a superconducting quantum interference device, Phys. Status Solidi B **246**, 2568 (2009).

[10] J. Voutilainen, M. A. Laakso, and T. T. Heikkilä, Physics of proximity josephson sensor, J. Appl. Phys. **107**, 064508 (2010).

[11] X. Du, D. E. Prober, H. Vora, and C. B. Mckitterick, Graphene-based bolometers, Graphene 2D Mater. **1**, 2299 (2014).

[12] H. B. Heersche, P. Jarillo-Herrero, J. B. Oostinga, L. M. Vandersypen, and A. F. Morpurgo, Bipolar supercurrent in graphene, Nature (London) **446**, 56 (2007).

[13] X. Du, I. Skachko, and E. Y. Andrei, Josephson current and multiple andreev reflections in graphene sns junctions, Phys. Rev. B **77**, 184507 (2008).

[14] F. Miao, S. Wijeratne, Y. Zhang, U. C. Coskun, W. Bao, and C. N. Lau, Phase-coherent transport in graphene quantum billiards, Science **317**, 1530 (2007).

[15] Y. Jiang, D.-X. Yao, E. W. Carlson, H.-D. Chen, and J. P. Hu, Andreev conductance in the $d + id'$-wave superconducting states of graphene, Phys. Rev. B **77**, 235420 (2008).

[16] C. Honerkamp, Density Waves and Cooper Pairing on the Honeycomb Lattice, Phys. Rev. Lett. **100**, 146404 (2008).

[17] A. M. Black-Schaffer and S. Doniach, Resonating valence bonds and mean-field d-wave superconductivity in graphite, Phys. Rev. B **75**, 134512 (2007).

[18] S. Pathak, V. B. Shenoy, and G. Baskaran, Possible high-temperature superconducting state with a $d + id$ pairing symmetry in doped graphene, Phys. Rev. B **81**, 085431 (2010).

[19] T. Ma, Z. Huang, F. Hu, and H.-Q. Lin, Pairing in graphene: A quantum monte carlo study, Phys. Rev. B **84**, 121410 (2011).

[20] C. W. J. Beenakker, Colloquium: Andreev reflection and Klein tunneling in graphene, Rev. Mod. Phys. **80**, 1337 (2008).

[21] A. Shailos, W. Nativel, A. Kasumov, C. Collet, M. Ferrier, S. Guéron, R. Deblock, and H. Bouchiat, Proximity effect and multiple Andreev reflections in few-layer graphene, Europhys. Lett. **79**, 57008 (2007).

[22] C. Ojeda-Aristizabal, M. Ferrier, S. Guéron, and H. Bouchiat, Tuning the proximity effect in a superconductor-graphene-superconductor junction, Phys. Rev. B **79**, 165436 (2009).

[23] M. Titov and C. W. J. Beenakker, Josephson effect in ballistic graphene, Phys. Rev. B **74**, 041401(R) (2006).

[24] J. G. Lambert, S. A. Carabello, and R. C. Ramos, Analysis of possible quantum metastable states in ballistic graphene-based josephson junctions, IEEE Trans. Appl. Supercond. **21**, 734 (2011).

[25] I. Hagymási, A. Kormányos, and J. Cserti, Josephson current in ballistic superconductor-graphene systems, Phys. Rev. B **82**, 134516 (2010).

[26] E. L. Pankratov and B. Spagnolo, Optimization of impurity profile for p-n-junction in heterostructures, Eur. Phys. J. B **46**, 15 (2005).

[27] S. S. Kubakaddi, Interaction of massless Dirac electrons with acoustic phonons in graphene at low temperatures, Phys. Rev. B **79**, 075417 (2009).

[28] W.-K. Tse and S. Das Sarma, Energy relaxation of hot Dirac fermions in graphene, Phys. Rev. B **79**, 235406 (2009).

[29] R. Bistritzer and A. H. MacDonald, Electronic Cooling in Graphene, Phys. Rev. Lett. **102**, 206410 (2009).

[30] J. K. Viljas and T. T. Heikkilä, Electron-phonon heat transfer in monolayer and bilayer graphene, Phys. Rev. B **81**, 245404 (2010).

[31] A. Betz, S. H. Jhang, E. Pallecchi, R. Ferreira, G. Fève, J.-M. Berroir, and B. Plaçais, Supercollision cooling in undoped graphene, Nat. Phys. **9**, 109 (2013).

[32] H. Suzuura and T. Ando, Phonons and electron-phonon scattering in carbon nanotubes, Phys. Rev. B **65**, 235412 (2002).

[33] M. I. Katsnelson, *Graphene: Carbon in Two Dimensions* (Cambridge University Press, Cambridge, 2012).

[34] J.-H. Chen, C. Jang, S. Xiao, M. Ishigami, and M. S. Fuhrer, Intrinsic and extrinsic performance limits of graphene devices on SiO_2, Nat. Nanotechnol. **3**, 206 (2008).

[35] D. K. Efetov and P. Kim, Controlling Electron-Phonon Interactions in Graphene at Ultrahigh Carrier Densities, Phys. Rev. Lett. **105**, 256805 (2010).

[36] N. Mizuno, B. Nielsen, and X. Du, Ballistic-like supercurrent in suspended graphene Josephson weak links, Nat. Commun. **4**, 2716 (2013).

[37] F. Miao, W. Bao, H. Zhang, and C. N. Lau, Premature switching in graphene josephson transistors, Solid State Commun. **149**, 1046 (2009).

[38] U. C. Coskun, M. Brenner, T. Hymel, V. Vakaryuk, A. Levchenko, and A. Bezryadin, Distribution of Supercurrent Switching in Graphene Under the Proximity Effect, Phys. Rev. Lett. **108**, 097003 (2012).

[39] C. English, D. Hamilton, C. Chialvo, I. Moraru, N. Mason, and D. V. Harlingen, Observation of non-sinusoidal current-phase relation in graphene Josephson junctions, arXiv:1305.0327.

[40] G.-H. Lee, S. Kim, S.-H. Jhi, and H.-J. Lee, Ultimately short ballistic vertical graphene josephson junctions, Nat. Commun. **6**, 6181 (2015).

[41] B. D. Josephson, Possible New Effects in Superconductive Tunnelling, Phys. Lett. **1**, 251 (1962).

[42] B. D. Josephson, The discovery of tunnelling supercurrents, Rev. Mod. Phys. **46**, 251 (1974).

[43] P. Reimann, C. Van den Broeck, H. Linke, P. Hänggi, J. M. Rubi, and A. Pérez-Madrid, Giant Acceleration of Free Diffusion by Use of Tilted Periodic Potentials, Phys. Rev. Lett. **87**, 010602 (2001).

[44] A. A. Dubkov and B. Spagnolo, Acceleration of diffusion in randomly switching potential with supersymmetry, Phys. Rev. E **72**, 041104 (2005).

[45] D. Jeong, J.-H. Choi, G.-H. Lee, S. Jo, Y.-J. Doh, and H.-J. Lee, Observation of supercurrent in pbin-graphenepbin josephson junction, Phys. Rev. B **83**, 094503 (2011).

[46] G.-H. Lee, D. Jeong, J.-H. Choi, Y.-J. Doh, and H.-J. Lee, Electrically Tunable Macroscopic Quantum Tunneling in a Graphene-Based Josephson Junction, Phys. Rev. Lett. **107**, 146605 (2011).

[47] J.-H. Choi, G.-H. Lee, S. Park, D. Jeong, J.-O. Lee, H.-S. Sim, Y.-J. Doh, and H.-J. Lee, Complete gate control of supercurrent in graphene p–n junctions, Nat. Commun. **4**, 2525 (2013).

[48] A. Barone and G. Paterno, *Physics and Applications of the Josephson Effect* (Wiley, New York, 1982).

[49] K. Likharev, *Dynamics of Josephson Junctions and Circuits* (Gordon & Breach, New York, 1986).

[50] A. L. Pankratov and B. Spagnolo, Suppression of Timing Errors in Short Overdamped Josephson Junctions, Phys. Rev. Lett. **93**, 177001 (2004).

[51] A. V. Gordeeva and A. L. Pankratov, Minimization of timing errors in reproduction of single flux quantum pulses, Appl. Phys. Lett. **88**, 022505 (2006).

[52] A. V. Gordeeva and A. L. Pankratov, Minimization of thermal jitter in a balanced comparator single flux quantum cell, J. Appl. Phys. **103**, 103913 (2008).

[53] G. Augello, D. Valenti, and B. Spagnolo, Effects of colored noise in short overdamped josephson junction, Int. J. Quantum Inf. **6**, 801 (2008).

[54] A. V. Gordeeva, A. L. Pankratov, and B. Spagnolo, Noise induced phenomena in point josephson junctions, Int. J. Bifurcation Chaos Appl. Sci. Eng. **18**, 2825 (2008).

[55] K. G. Fedorov and A. L. Pankratov, Mean time of the thermal escape in a current-biased long-overlap josephson junction, Phys. Rev. B **76**, 024504 (2007).

[56] K. G. Fedorov, A. L. Pankratov, and B. Spagnolo, Influence of length on the noise delayed switching of long josephson junctions, Int. J. Bifurcation Chaos Appl. Sci. Eng. **18**, 2857 (2008).

[57] K. G. Fedorov and A. L. Pankratov, Crossover of the Thermal Escape Problem in Annular Spatially Distributed Systems, Phys. Rev. Lett. **103**, 260601 (2009).

[58] G. Augello, D. Valenti, A. L. Pankratov, and B. Spagnolo, Lifetime of the superconductive state in short and long josephson junctions, Eur. Phys. J. B **70**, 145 (2009).

[59] D. Valenti, C. Guarcello, and B. Spagnolo, Switching times in long-overlap josephson junctions subject to thermal fluctuations and non-gaussian noise sources, Phys. Rev. B **89**, 214510 (2014).

[60] G. Augello, D. Valenti, and B. Spagnolo, Non-gaussian noise effects in the dynamics of a short overdamped josephson junction, Eur. Phys. J. B **78**, 225 (2010).

[61] Y. Yu and S. Han, Resonant Escape Over an Oscillating Barrier in Underdamped Josephson Tunnel Junctions, Phys. Rev. Lett. **91**, 127003 (2003).

[62] G. Sun, N. Dong, G. Mao, J. Chen, W. Xu, Z. Ji, L. Kang, P. Wu, Y. Yu, and D. Xing, Thermal escape from a metastable state in periodically driven josephson junctions, Phys. Rev. E **75**, 021107 (2007).

[63] C. Pan, X. Tan, Y. Yu, G. Sun, L. Kang, W. Xu, J. Chen, and P. Wu, Resonant activation through effective temperature oscillation in a josephson tunnel junction, Phys. Rev. E **79**, 030104(R) (2009).

[64] H. Grabert, Theory of a josephson junction detector of non-gaussian noise, Phys. Rev. B **77**, 205315 (2008).

[65] D. F. Urban and H. Grabert, Feedback and rate asymmetry of the josephson junction noise detector, Phys. Rev. B **79**, 113102 (2009).

[66] J. Ankerhold, Detecting Charge Noise with a Josephson Junction: A Problem of Thermal Escape in Presence of Non-Gaussian Fluctuations, Phys. Rev. Lett. **98**, 036601 (2007).

[67] E. V. Sukhorukov and A. N. Jordan, Stochastic dynamics of a josephson junction threshold detector, Phys. Rev. Lett. **98**, 136803 (2007).

[68] M. Köpke and J. Ankerhold, Linear dynamics subject to thermal fluctuations and non-gaussian noise: From classical to quantum, New J. Phys. **15**, 043013 (2013).

[69] G. Filatrella and V. Pierro, Detection of noise-corrupted sinusoidal signals with josephson junctions, Phys. Rev. E **82**, 046712 (2010).

[70] P. Addesso, G. Filatrella, and V. Pierro, Characterization of escape times of josephson junctions for signal detection, Phys. Rev. E **85**, 016708 (2012).

[71] P. Addesso, V. Pierro, and G. Filatrella, Escape time characterization of pendular fabry-perot, Europhys. Lett. **101**, 20005 (2013).

[72] P. Addesso, G. Filatrella, and V. Pierro, Escape time of josephson junctions for signal detection, in *Spontaneous Symmetry Breaking, Self-Trapping, and Josephson Oscillations*, Progress in Optical Science and Photonics, Vol. 1, edited by B. A. Malomed (Springer, Berlin, Heidelberg, 2013), pp. 657–678.

[73] V. Pierro and G. Filatrella, Fabryperot filters with tunable josephson junction defects, Physica C **517**, 37 (2015).

[74] K. Lindenberg, J. M. Sancho, A. M. Lacasta, and I. M. Sokolov, Dispersionless transport in a washboard potential, Phys. Rev. Lett. **98**, 020602 (2007).

[75] P. Hänggi and F. Marchesoni, Artificial Brownian motors: Controlling transport on the nanoscale, Rev. Mod. Phys. **81**, 387 (2009).

[76] O. M. Braun, R. Ferrando, and G. E. Tommei, Stimulated diffusion of an adsorbed dimer, Phys. Rev. E **68**, 051101 (2003).

[77] P. Tierno, P. Reimann, T. H. Johansen, and F. Sagués, Giant Transversal Particle Diffusion in a Longitudinal Magnetic Ratchet, Phys. Rev. Lett. **105**, 230602 (2010).

[78] C. Dalle-Ferrier, M. Kruger, R. D. L. Hanes, S. Walta, M. C. Jenkins, and S. U. Egelhaaf, Dynamics of dilute colloidal suspensions in modulated potentials, Soft Matter **7**, 2064 (2011).

[79] G. Tatara, N. Vernier, and J. Ferré, Universality of thermally assisted magnetic domain-wall motion under spin torque, Appl. Phys. Lett. **86**, 252509 (2005).

[80] R. A. Duine, A. S. Núñez, and A. H. MacDonald, Thermally assisted current-driven domain-wall motion, Phys. Rev. Lett. **98**, 056605 (2007).

[81] J. Xing, H. Wang, and G. Oster, From continuum fokker-planck models to discrete kinetic models, Biophys. J. **89**, 1551 (2005).

[82] B. Lisowski, D. Valenti, B. Spagnolo, M. Bier, and E. Gudowska-Nowak, Stepping molecular motor amid lévy white noise, Phys. Rev. E **91**, 042713 (2015).

[83] S. A. Tatarkova, W. Sibbett, and K. Dholakia, Brownian particle in an optical potential of the washboard type, Phys. Rev. Lett. **91**, 038101 (2003).

[84] M. Šiler and P. Zemánek, Particle jumps between optical traps in a one-dimensional (1d) optical lattice, New J. Phys. **12**, 083001 (2010).

[85] B. J. Lopez, N. J. Kuwada, E. M. Craig, B. R. Long, and H. Linke, Realization of a Feedback Controlled Flashing Ratchet, Phys. Rev. Lett. **101**, 220601 (2008).

[86] I. Bonnet and P. Desbiolles, The diffusion constant of a labeled protein sliding along dna, Eur. Phys. J. E **34**, 25 (2011).

[87] E. R. Kay, D. A. Leigh, and F. Zerbetto, Synthetic molecular motors and mechanical machines, Angew. Chem., Int. Ed. Engl. **46**, 72 (2007).

[88] A. Ros, R. Eichhorn, J. Regtmeier, T. T. Duong, P. Reimann, and D. Anselmetti, Brownian motion: Absolute negative particle mobility, Nature (London) **436**, 928 (2005).

[89] P. G. de Gennes, *Superconductivity of Metals and Alloys* (Benjamin, New York, 1966).

[90] P. Brouwer and C. Beenakker, Anomalous temperature dependence of the supercurrent through a chaotic josephson junction, Chaos Solitons Fractals **8**, 1249 (1997).

[91] J. Tworzydło, B. Trauzettel, M. Titov, A. Rycerz, and C. W. J. Beenakker, Sub-poissonian shot noise in graphene, Phys. Rev. Lett. **96**, 246802 (2006).

[92] I. Hagymási (private communication). Figure 1(a) of Ref. [25] shows data only for $T/T_c = 0,0.53,0.71$. The proof regarding the temperature-independent behavior of $i(\varphi)$ for $T/T_c \lesssim 0.25$ is the result of private communication with the author.

[93] J. Männik, S. Li, W. Qiu, W. Chen, V. Patel, S. Han, and J. E. Lukens, Crossover from Kramers to phase-diffusion switching in moderately damped josephson junctions, Phys. Rev. B **71**, 220509 (2005).

[94] V. M. Krasnov, T. Bauch, S. Intiso, E. Hürfeld, T. Akazaki, H. Takayanagi, and P. Delsing, Collapse of thermal activation in moderately damped josephson junctions, Phys. Rev. Lett. **95**, 157002 (2005).

[95] H. Grabert and U. Weiss, Crossover from Thermal Hopping to Quantum Tunneling, Phys. Rev. Lett. **53**, 1787 (1984).

[96] C. W. Gardiner, *Handbook of Stochastic Methods for Physics, Chemistry, and the Natural Sciences* (Springer-Verlag, Berlin, 2004), p. 106.

[97] N. V. Agudov and B. Spagnolo, Noise-enhanced stability of periodically driven metastable states, Phys. Rev. E **64**, 035102(R) (2001).

[98] A. A. Dubkov, N. V. Agudov, and B. Spagnolo, Noise-enhanced stability in fluctuating metastable states, Phys. Rev. E **69**, 061103 (2004).

[99] C. R. Doering and J. C. Gadoua, Resonant activation over a fluctuating barrier, Phys. Rev. Lett. **69**, 2318 (1992).

[100] R. N. Mantegna and B. Spagnolo, Experimental investigation of resonant activation, Phys. Rev. Lett. **84**, 3025 (2000).

[101] R. N. Mantegna and B. Spagnolo, Numerical simulation of resonant activation in a fluctuating metastable model system, J. Phys. IV (France) **08**, Pr6-247 (1998).

[102] P. Pechukas and P. Hänggi, Rates of Activated Processes with Fluctuating Barriers, Phys. Rev. Lett. **73**, 2772 (1994).

[103] M. Marchi, F. Marchesoni, L. Gammaitoni, E. Menichella-Saetta, and S. Santucci, Resonant activation in a bistable system, Phys. Rev. E **54**, 3479 (1996).

[104] B. Dybiec and E. Gudowska-Nowak, Lévy stable noise-induced transitions: Stochastic resonance, resonant activation and dynamic hysteresis, J. Stat. Mech.: Theory Exp. (2009) P05004.

[105] S. Miyamoto, K. Nishiguchi, Y. Ono, K. M. Itoh, and A. Fujiwara, Resonant escape over an oscillating barrier in a single-electron ratchet transfer, Phys. Rev. B **82**, 033303 (2010).

[106] Y. Hasegawa and M. Arita, Escape process and stochastic resonance under noise intensity fluctuation, Phys. Lett. A **375**, 3450 (2011).

[107] A. Fiasconaro and B. Spagnolo, Resonant activation in piecewise linear asymmetric potentials, Phys. Rev. E **83**, 041122 (2011).

[108] D. Valenti, G. Augello, and B. Spagnolo, Dynamics of a FitzHugh-Nagumo system subjected to autocorrelated noise, Eur. Phys. J. B **65**, 443 (2008).

[109] C. Guarcello, D. Valenti, G. Augello, and B. Spagnolo, The role of non-Gaussian sources in the transient dynamics of long Josephson junctions, Acta Phys. Pol. B **44**, 997 (2013).
[110] M. H. Devoret, J. M. Martinis, D. Esteve, and J. Clarke, Resonant activation from the zero-voltage state of a current-biased Josephson junction, Phys. Rev. Lett. **53**, 1260 (1984).
[111] M. H. Devoret, J. M. Martinis, and J. Clarke, Measurements of Macroscopic Quantum Tunneling Out of the Zero-Voltage State of a Current-Biased Josephson Junction, Phys. Rev. Lett. **55**, 1908 (1985).
[112] J. M. Martinis, M. H. Devoret, and J. Clarke, Experimental tests for the quantum behavior of a macroscopic degree of freedom: The phase difference across a josephson junction, Phys. Rev. B **35**, 4682 (1987).
[113] C. Guarcello, D. Valenti, A. Carollo, and B. Spagnolo, Stabilization Effects of Dichotomous Noise on the Lifetime of the Superconducting State in a Long Josephson Junction , Entropy **17**, 2862 (2015).
[114] R. N. Mantegna and B. Spagnolo, Noise enhanced stability in an unstable system, Phys. Rev. Lett. **76**, 563 (1996).
[115] B. Spagnolo, N. Agudov, and A. Dubkov, Noise enhanced stability, Acta Phys. Pol. B **35**, 1419 (2004).
[116] P. D'Odorico, F. Laio, and L. Ridolfi, Noise-induced stability in dryland plant ecosystems, Proc. Natl. Acad. Sci. USA **102**, 10819 (2005).
[117] A. Fiasconaro, B. Spagnolo, and S. Boccaletti, Signatures of noise-enhanced stability in metastable states, Phys. Rev. E **72**, 061110 (2005).
[118] P. I. Hurtado, J. Marro, and P. L. Garrido, Metastability, nucleation, and noise-enhanced stabilization out of equilibrium, Phys. Rev. E **74**, 050101(R) (2006).
[119] B. Spagnolo, A. Dubkov, A. Pankratov, E. Pankratova, A. Fiasconaro, and A. Ochab-Marcinek, Lifetime of metastable states and suppression of noise in interdisciplinary physical models, Acta Phys. Pol. B **38**, 1925 (2007).
[120] R. Mankin, E. Soika, A. Sauga, and A. Ainsaar, Thermally enhanced stability in fluctuating bistable potentials, Phys. Rev. E **77**, 051113 (2008).
[121] M. Yoshimoto, H. Shirahama, and S. Kurosawa, Noise-induced order in the chaos of the belousov-zhabotinsky reaction, J. Chem. Phys. **129**, 014508 (2008).
[122] A. Fiasconaro and B. Spagnolo, Stability measures in metastable states with gaussian colored noise, Phys. Rev. E **80**, 041110 (2009).
[123] M. Trapanese, Noise enhanced stability in magnetic systems, J. Appl. Phys. **105**, 07D313 (2009).
[124] A. Fiasconaro, J. J. Mazo, and B. Spagnolo, Noise-induced enhancement of stability in a metastable system with damping, Phys. Rev. E **82**, 041120 (2010).
[125] J.-H. Li and J. Łuczka, Thermal-inertial ratchet effects: Negative mobility, resonant activation, noise-enhanced stability, and noise-weakened stability, Phys. Rev. E **82**, 041104 (2010).
[126] A. A. Smirnov and A. L. Pankratov, Influence of the size of uniaxial magnetic nanoparticle on the reliability of high-speed switching, Phys. Rev. B **82**, 132405 (2010).
[127] H. Kramers, Brownian motion in a field of force and the diffusion model of chemical reactions, Physica **7**, 284 (1940).
[128] V. Mel'nikov, The Kramers problem: Fifty years of development, Phys. Rep. **209**, 1 (1991).
[129] P. Hänggi, P. Talkner, and M. Borkovec, Reaction-rate theory: fifty years after Kramers, Rev. Mod. Phys. **62**, 251 (1990).
[130] J. E. Hirsch, B. A. Huberman, and D. J. Scalapino, Theory of intermittency, Phys. Rev. A **25**, 519 (1982).
[131] E. V. Pankratova, A. V. Polovinkin, and B. Spagnolo, Suppression of noise in FitzHugh-Nagumo model driven by a strong periodic signal, Phys. Lett. A **344**, 43 (2005).
[132] A. Fiasconaro, D. Valenti, and B. Spagnolo, Role of the initial conditions on the enhancement of the escape time in static and fluctuating potentials, Physica A **325**, 136 (2003).
[133] B. Spagnolo, A. Dubkov, and N. Agudov, Enhancement of stability in randomly switching potential with metastable state, Eur. Phys. J. B **40**, 273 (2004).
[134] N. V. Agudov, A. A. Dubkov, and B. Spagnolo, Escape from a metastable state with fluctuating barrier, Physica A **325**, 144 (2003).
[135] B. Spagnolo, P. Caldara, A. La Cognata, G. Augello, D. Valenti, A. Fiasconaro, A. Dubkov, and G. Falci, Relaxation phenomena in classical and quantum systems, Acta Phys. Pol. B **43**, 1169 (2012).
[136] R. N. Mantegna and B. Spagnolo, Probability distribution of the residence times in periodically fluctuating metastable systems, Int. J. Bifurcation Chaos Appl. Sci. Eng. **08**, 783 (1998).
[137] G. Bonanno, D. Valenti, and B. Spagnolo, Role of noise in a market model with stochastic volatility, Eur. Phys. J. B **53**, 405 (2006).
[138] D. Valenti, B. Spagnolo, and G. Bonanno, Hitting time distributions in financial markets, Physica A **382**, 311 (2007).
[139] G. Bonanno, D. Valenti, and B. Spagnolo, Mean escape time in a system with stochastic volatility, Phys. Rev. E **75**, 016106 (2007).
[140] N. Pizzolato, A. Fiasconaro, and B. Spagnolo, Noise effects in polymer dynamics, Int. J. Bifurcation Chaos Appl. Sci. Eng. **18**, 2871 (2008).
[141] N. Pizzolato, A. Fiasconaro, D. P. Adorno, and B. Spagnolo, Resonant activation in polymer translocation: New insights into the escape dynamics of molecules driven by an oscillating field, Phys. Biol. **7**, 034001 (2010).
[142] B. Spagnolo, S. Spezia, L. Curcio, N. Pizzolato, A. Fiasconaro, D. Valenti, P. Lo Bue, E. Peri, and S. Colazza, Noise effects in two different biological systems, Eur. Phys. J. B **69**, 133 (2009).
[143] T. Zhou, F. Moss, and P. Jung, Escape-time distributions of a periodically modulated bistable system with noise, Phys. Rev. A **42**, 3161 (1990).
[144] P. Jung, Periodically driven stochastic systems, Phys. Rep. **234**, 175 (1993).